Impact of tectonic shortening on fluid overpressure in petroleum system modelling : Insights from the Neuquén basin, Argentina

J. Berthelon, A. Brüch, D. Colombo, J. Frey, R. Traby, A. Bouziat, M.C. C Cacas-Stentz, T. Cornu

Impact of tectonic shortening on fluid overpressure in petroleum system modelling: insights from the Neuquén basin, Argentina.

J. Berthelon[1], A. Brüch[1], D. Colombo[1], J. Frey[1], R. Traby[2], A. Bouziat[1], M.C. Cacas-Stentz[1], T. Cornu[3]

1: IFP Energies nouvelles, 1 et 4 avenue de Bois-Préau, 92852 Rueil-Malmaison, France

2: Total Exploration and Production, Paris La Défense, F-92078, France

3: Total Exploration and Production, R&D, CSTJF, Pau, France

Abstract

Petroleum System Modelling (PSM) is a method which reproduces the burial history of sedimentary basins, together with rock properties, thermal and stress state, fluid flow and chemical transfers. The Vaca-Muerta Formation (Fm) in the Neuquén foreland basin, Argentina, presents exceptionally high overpressure despite the latest erosional history coeval with the current basin shortening. PSM currently accounts for vertical compaction laws only, which are not sufficient to match the observed pore pressure while keeping permeability values realistic. It also prevents to discuss the relationships between natural fracturing and the basin hydrodynamic. To assess these phenomena, a code coupling a PSM and a geomechanical simulator is used, in which we consider a 3D poro-elastoplastic geomechanical framework that accounts for both burial and tectonic compaction. Using this coupled approach, we calibrate porosity and pore pressure in a 3D geological model of the Neuquén basin using successives tectonic shortening phases related to the Andean subduction. Compared to PSM results using similar parameters, this study quantifies how much Andean tectonic deformation influenced pore pressure evolution in the basin. It shows that Late Miocene to recent tectonic could explain most of the overpressure observed in the Vaca-Muerta Fm. A shear-induced fracturing index provided by the constitutive model suggests that fracturing in the Vaca-Muerta Fm is very likely to occur during one of the main Andean deformation phases. The work suggests that pore pressure prediction in regions that have been subjected to lateral tectonic loading should be handled considering a 3D geomechanical approach. Using the Neuquén basin as an example, the present study discusses the impact of tectonic in pore pressure evolution, and its role in natural fluid migration in sedimentary basins subjected to tectonic deformation.

Keywords

Sedimentary basin, Fluid overpressure, Neuquén basin, seal rock fracturing, geomechanics, numerical modelling

Highlights

- We couple a basin and petroleum system code and a geomechanical code to model tectonic shortening in the poro-mechanichal evolution of the Neuquén basin
- Miocene to recent Andean tectonics can explain most of the present-day fluid overpressure in the Vaca-Muerta Fm.
- The Vaca-Muerta Fm seal fracturing occurs simultaneously to the Andean deformation phases.

Article

1. Introduction

Pore pressure is a key physical variable of sedimentary basins, as its distribution strongly influences the basin structural evolution (Hubbert and Rubey, 1959; Mourgues and Cobbold, 2003) and migration of fluids (England et al., 1987; Hantschel and Kauerauf, 2009). Its prediction is critical for many sub-surface industrial applications, as it is used to minimize drilling costs and risks (Zoback, 2010). It also provides valuable information on fluid migration pathways, reservoir quality and seal capacity. In particular, natural fracturing of reservoirs and seals is often related to phases of overpressure (Lorenz et al., 1991; Sibson, 2003; Roure et al, 2005), and has considerable influence on the hydraulic transfer properties of sedimentary rocks. Petroleum System Modelling (PSM) is one of the methods made available to assess pore pressure history, as it simulates most of the physical and chemical processes controlling overpressure during basin geological history (Schneider et al., 2000; Tuncay and Orteleva, 2004; Hantschel and Kauerauf, 2009). This tool allows one to test different scenario under which overpressure is developed, and how it is subsequently dissipated and redistributed across the basin, thus affecting fluid migration and seal integrity.

However, the model classically used in this approach is limited because it calculates mechanical compaction from the sediment weight only, therefore considering only vertical effective stress. There are several geological cases where horizontal loading significantly contributes to overpressure development and seal fracturing (Osborne and Swarbrick, 1997; Obradors-Prat et al, 2017; Bouziat et al, 2019). In tectonically active basins for instance, the horizontal effective stresses may approach or even exceed the vertical effective stress (Zoback et al., 1989). In foreland basin in particular, it has been shown that Layer-Parallel-Shortening (LPS) resulting from far-field compression considerably deform the sedimentary rocks (Robion et al, 2007; Tavani et al., 2015), leading to observable porosity decrease (Couzens-Schultz and Azbel, 2014). This early tectonic contraction phase partly controls migration of natural fluids in forelands and Fold-and-Thrust Belts (FTB) (Roure et al., 2005, 2010). Therefore, in such geological contexts, classical PSM methods can bring to inaccurate pore pressure estimates and fluid circulation assessment (Burgreen-Chan et al., 2016; Neumaier et al., 2014; Obradors-Prat et al, 2017).

In order to quantitatively assess the consequences of this one-dimensional simplified approach, we focus on the Neuquén basin, Argentina, in which discoveries of unconventional oil and gas resources in the Vaca-Muerta shale rocks sparked a renewed interest. This region of the Central Andes experienced intraplate deformations from the Upper Cretaceous to the Mio-Pliocene (Horton, 2018). High overpressure that may reach 90% of the lithostatic stress is measured in the Vaca-Muerta Formation (Fm) (Badessich et al., 2016), despite the low sedimentation rates prevailing since the Paleogene and the latest erosional history coeval with the ongoing basin shortening (Zamora-Valcarce et al, 2006). In this foreland basin, classical PSM using a 1D compaction model appears unable to explain the observed pore pressure except by unrealistic permeabilities, which also prevents to discuss the relationship between natural fracturing and the basin hydrodynamic. It suggests that, among other processes, lateral compaction resulting from the Andean tectonic shortening may have a role to play in the overpressure development of the Neuquén basin.

In this work, we simulate the Neuquén embayement and Chihuidos regions history since the Lower Jurassic with a code coupling a PSM and a geomechanical simulator in order to remove the limitations of the 1D compaction hypothesis. Our objective here is to evaluate the effects of a 3D compaction model with respect to a 1D model, in order to assess how tectonic history controls fluid pressure and rock properties. After a brief description of the classical PSM approach and of the iterative coupling strategy, the geological settings of the Neuquén basin is presented. Then, the model set-up is described, including the 3D geological model architecture, the structural evolution, the thermal and poro-mechanical parameters used and the applied boundary conditions. Results obtained from both the coupled model and the classical PSM using the same settings are compared in order to discuss the impact of 3D geomechanics in pore pressure modelling. The coupled simulation is then taken as the reference model for further developments, including the analysis of shear-induced fracturing and assessment of natural fracture distribution over the basin. Finally, we discuss the impact of far-field tectonics during LPS phase on the pore pressure evolution of the Neuquén foreland basin.

2. Geological settings

The geological history of the Central Andes involves several tectonic, sedimentary and volcanic cycles, resulting in a complex present-day morphotectonic configuration (Vergani et al, 1995; Ramos & Folguera, 2005; Ramos & Kay, 2006). Episodic deformation phases since the Mesozoic have been

attributed to cyclic changes in the long-lived Andean subduction system, attesting to margin-wide plate tectonic reorganizations and slab-mantle interactions (Chen et al, 2019). The Neuquén basin corresponds to a triangular segment of the Andes foreland, located within the retro-arc of the southern central Andes, between 32°S and 41°S (Figure 1).

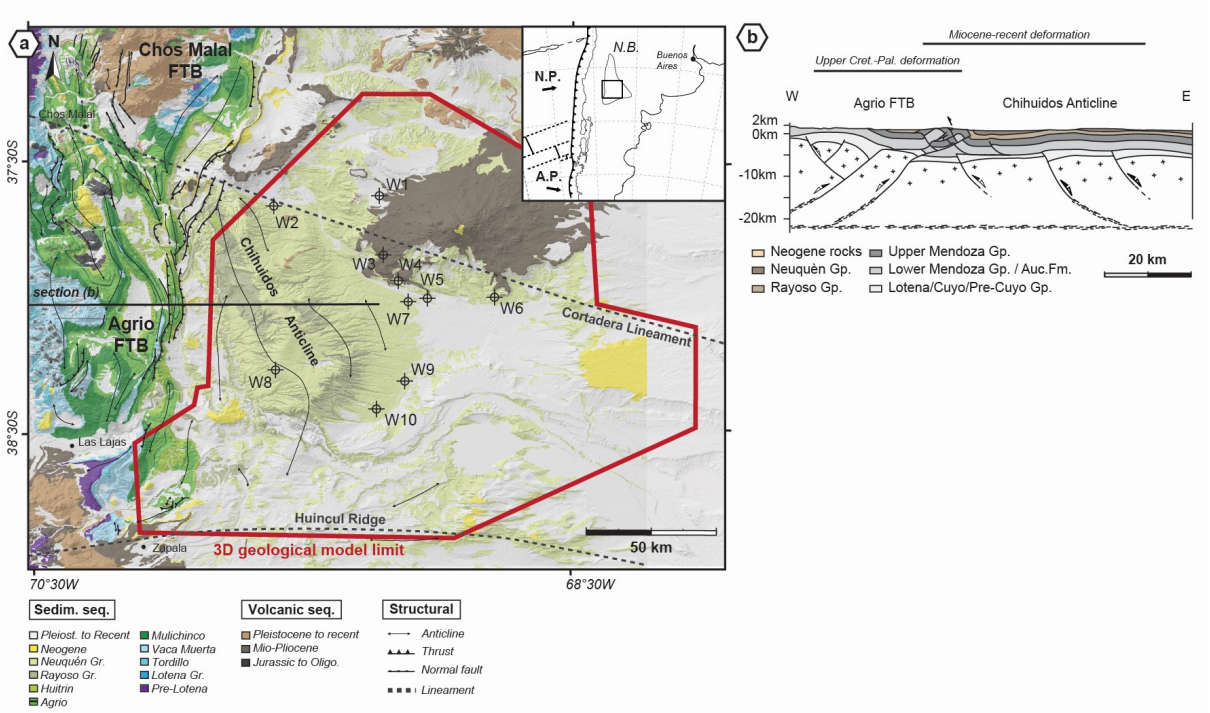

Figure 1: Structural and sedimentary architecture of the southern Neuquén basin. (a) Geological map of the Neuquén basin, modified from SEGEMAR 1/200 000 geological maps, and extent of the 3D model. Localisation of the map in the Southern American continent is provided in the insert. N.P.: Nazca Plate, A.P.; Antartica Plate, N.B.: Neuquén basin. (b) Schematic structural section across the Agrio FTB and adjacent folded foreland, modified from Zamora-Valcare et al, 2006.

Our study focuses on the southern part of the Neuquén basin (Figure 1a). In this region, Paleozoic basement rocks were affected by a rifting episode during the Late Triassic, leading to the formation of NW-SE trending half-grabens infilled by the Pre-Cuyo group (Figure 2). From the Jurassic to the lower Cretaceous, back-arc thermal subsidence leads to the alternate deposition of marine and continental rocks. The Cuyo Group deposition starts during the lower Jurassic (Leanza et al, 2013), and is notably composed of the Los Molles Formation (Fm), a thick formation composed of black shales interbedded with turbiditic sequences. The Lajas Fm and Punta Rosada Fm, composed of marine and deltaic sediments, mark the end of the Cuyo Group (Arregui et al, 2011). A transgression episode from

Middle Callovian to Late Oxfordian (165 Ma to 155 Ma) led to the deposition of the Lotena Group (Legarreta and Gulisano, 1989). It comprises the limestones of the La Manga Fm, overlaid by the 100m thick evaporitic layer of the Aucquilco Fm (Figure 2). The Mendoza Group represents the most important and best exposed group in the Neuquén basin (Figure 1a). It starts with the continental deposits of fluvial and aeolian origin of the Tordillo Fm at the Kimmeridgian-Tithonian transition (Naipauer et al, 2015), which unconformably overly the Lotena Group deposits. This formation strongly thickens westward, from 50 m to 700 m approximately.

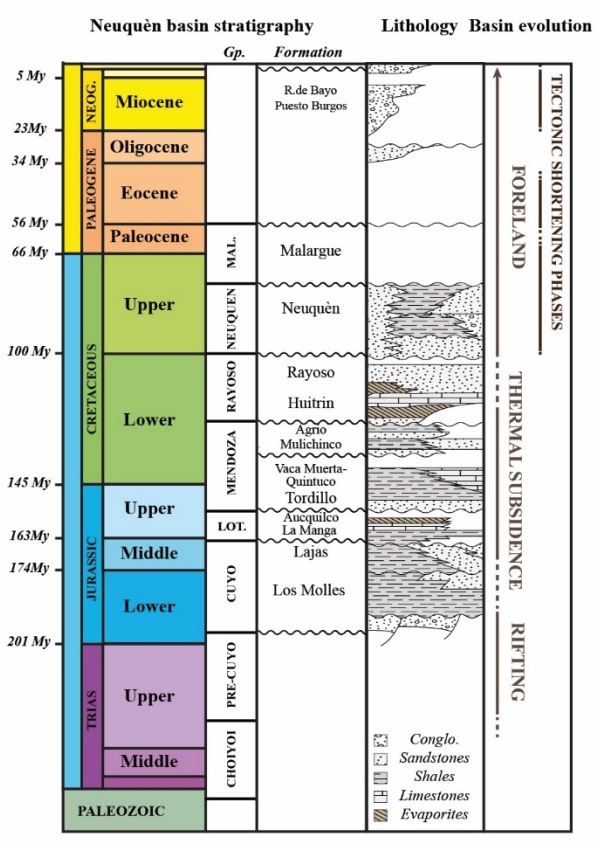

Figure 2: Lithostratigraphic chart of the southern part of the Neuquén basin, modified from Messager et al (2010) and Rojas Vera et al (2015). Lithology and basin evolution are modified from Cobbold and Rosselo (2003), Zamora-Valcarce et al (2006), Zamora-Valcarce (2007) and Sánchez et al (2018).

It is overlain by the Vaca Muerta-Quintuco Fm, which ranges from Tithonian to Lower Valanginian age (Leanza et al, 2011; Kietzman et al, 2016). This formation represents the main hydrocarbon source-rock of the Neuquén basin as well as an excellent unconventional reservoir. The Vaca Muerta-

Quintuco Fm is a thick shallowing upward sedimentary sequence, consisting of black shales, marlstones, limestones and bioclastic siltstones (Legarreta and Uliana, 1996), in which the Quintuco Member represents carbonates facies in shallow platform depositional environment (Kietzmann et al, 2016). On top of this unit, the Valanginian Mulichinco Fm is deposited during a sudden relative sea-drop, leading to the deposition of continental to marine sandstones (Schwartz and Howell, 2005). It progressively transitions to the thick marine black shales and interbedded limestones deposits which constitutes the Valanginian-Barremian Agrio Fm (Spalletti et al, 2011). The overlying Bajada del Agrio Group is composed of two sub-units. The Huitrin Fm consists of fluvial-aeolian sandstones, limestones and evaporites (Leanza, 2003). The Aptian-Albian Rayoso Fm contains dominantly reddish fluvial and lacustrine deposits (Zavala and Ponce, 2011), and marks the disconnection of the Neuquén basin with the proto-Pacific ocean. During the Upper Cretaceous, the Neuquén basin evolved into a foreland basin, following the initiation of the Nazca plate subduction (Horton, 2018). A regional unconformity separates the Neuquén Group from the Mendoza Group (Figure 2), whose base is dated at 99 Ma (Tunik et al, 2010). This group is composed by thick continental clastic sequences, mainly sandstones, minor conglomerates and shales. Almost all the outcropping rocks located east of the FTBs consist of sediments from the Neuquén Group (Figure 1a). From the Campanian to the Paleocene, an Atlantic transgression led to the unconformable deposition of the Malargue Group on top of the Neuquén Group. These deposits mainly consist of continental and marine sedimentary succession (Rodriguez et al, 2011). A very sparse sedimentation characterizes the Neuquén basin since the end of the Paleocene (Zapata and Folguera, 2005; Zamora Valcarce et al, 2009; Rojas Vera et al, 2015). Beyond the frontal thrust only a few patches of syn-orogenic Miocene to Pleistocene continental deposits remain, mainly consisting of remnant terraces and alluvial deposits (Zamora-Valcarce et al, 2006; Messager et al, 2010).

The structural architecture of the Neuquén basin shows the transition from the FTB domain to the folded foreland to the gently deformed foreland (Figure 1). The Chihuidos Anticline forms the major structure in the model extent, and consists of a large wavelength anticline, probably resulting from the inversion of a deeply rooted half-graben (Mosquera and Ramos, 2006; Figure 1b). The NW-SE Cortaderas Lineament corresponds to the boundary separating the northern Chos-Malal FTB and the southern Agrio FTB. Still, this structural feature does not have any straightforward expression into the sedimentary pile of the foreland basin. Successive shortening phases since the Upper Cretaceous led

to basin inversion with mixed thin-skinned and thick-skinned tectonics (Vergani et al, 1995; Zapata and Folguera, 2005; Zamora-Valcarce et al, 2006; Figure 1b). FTBs development progressively migrates toward the foreland during these phases. Andean deformation started at 100-88 Ma in the Neuquén basin (Tunik et al, 2010; Di Giulio et al, 2012), and is associated in the study area with the uplift of the Cordillera del Viento, west of the Chos Malal FTB, and the inner part of the Chos Malal and Agrio FTBs (Rojas Vera et al, 2015; Sánchez et al, 2018). Upper Cretaceous-Paleocene deformation led to significantly shorten the inner part of both FTBs (Cobbold and Rosselo, 2003; Zapata & Folguera, 2005; Zamora-Valcarce et al, 2006; Rojas Vera et al, 2015, Fennel et al, 2020). It remains however unclear how much of the displacement currently observed on the frontal structures have been acquired at that time. After a period of tectonic quiescence during the Paleogene, tectonic deformation resumes during the Miocene (Zapata & Folguera, 2005; Ramos & Kay, 2006), which led to the reactivation of the frontal structures and the propagation of back-thrusts in the FTB. Most authors point to a polyphased history to explain the shortening of the frontal structures, and suggest that they result from Miocene thick-skinned deformations of anterior thin-skinned deformations (Zamora-Valcarce and Zapata, 2015; Rojas Vera et al, 2015; Sánchez et al, 2018; Lebinson et al, 2018; Fennel et al, 2020). While most assume a Miocene age for the late thick-skinned deformations, the early thin-skinned deformations are either related to the same Neogene event (Rojas Vera et al, 2015; Sánchez et al; 2018; Lebinson et al, 2018) or the Upper Cretaceous-Paleocene one (Zamora Valcarce et al, 2006). It is suggested that the Chihuidos Anticline dominantly uplifts during the Neogene (Zamora Valcarce et al, 2009; Rojas Vera et al, 2015), while it continuously but more slowly uplifts until present-day (Messager et al, 2010).

3. Method and data

3.1 : Method: PSM and 3D geomechanical coupled simulations

PSM is becoming a more and more standard tool to simulate the evolution of sedimentary basins (Hantschel and Kauerauf, 2009). It adopts a forward simulation which simulates the full history of the basin development starting from the deposition of the oldest layer and proceeding until the entire sequence of sedimentary layers has been deposited and the present-day geometry is reached. Prior to forward modelling, the sedimentary basin geometry is restored through geological ages with a

backward process, using simple backstripping when lateral deformation and displacements can be neglected (Perrier and Quiblier, 1974) or true structural restoration otherwise (Neumaier et al, 2014; Burgreen-Chan et al, 2016; Woillez et al, 2017). Based on a space and time discretization of the basin in 3D cells and geological events, it delivers a quantitative prediction of variables evolving through space and time, including pressure, porosity, temperature, hydrocarbon generation and migration. Physical and mathematical concepts behind these calculations are extensively described in Schneider et al (2000) and Hantschel and Kauerauf (2009).

Overpressure in PSM is principally due to disequilibrium compaction since porosity and permeability are directly linked (e.g. Luijendijk and Gleeson, 2015). Vertical loading from burial is usually considered as the predominant factor controlling rock compaction. Therefore, a 1D vertical geomechanical modelling is embedded in PSM. Various compaction models have been used in this context, such as those proposed by Schneider et al (1996). These phenomenological laws usually describe porosity as an exponential function of vertical effective stress. Regarding to PSM, the assumption that compaction is only driven by vertical processes can be limiting, especially in compressive geological contexts where important part of the loading can be associated with tectonic shortening (Osborne and Swarbrick, 1997).

To overcome the limitation of classical PSM regarding the absence of lateral deformation, an iterative coupling strategy between a PSM simulator (Faille et al, 2014) and a 3D mechanical finite element code (Code_Aster, http://www.code-aster.org) had been developped to perform basin-scale simulations. In this approach, the consistency of porosities evaluated from both the geomechanical model and the PSM is checked at the end of each geological events (Figure 3). During these periods, each code has its own time discretization and independent porosity evaluation. If the difference between the two porosities is not negligible, porosity and/or pressure is iteratively corrected in the PSM and the time event is computed again until convergence is reached (Brüch et al, 2020). A similar approach is also used for geomechanical coupling in reservoir simulations (Mainguy and Longuemarre, 2002). The coupled simulation account for a 3D poro-mechanical framework by means of a poro-elastoplastic constitutive law (Brüch et al, 2020). The yield surface corresponds to the modified Cam-Clay model (Wood, 1990) in which the consolidation pressure represents the hardening parameter of the model and depends on the material porosity. The hardening law is adapted to

reproduce porosity trends as those given by the Schneider law when submitted to oedometric conditions, which ensure that without active tectonics the porosity evolution follows those of classical PSM simulator. Therefore, lateral compaction is not calculated by the structural restoration, but during the forward simulation. In this regard, the geometrical consistency between the backward structural restoration and the forward coupled simulation is beyond the scope of this study. We neglect overpressure mechanisms other than stress-related ones, such as kerogen transformation for instance (Swarbrick et al, 2001), in order to focus on the analysis of the impact of lateral loading. It means that the only overpressure mechanisms made possible in this work are the disequilibrium compaction resulting from ineffective dewatering and/or lateral transfer through permeable rock bodies (as in Yardley & Swarbrick, 2000).

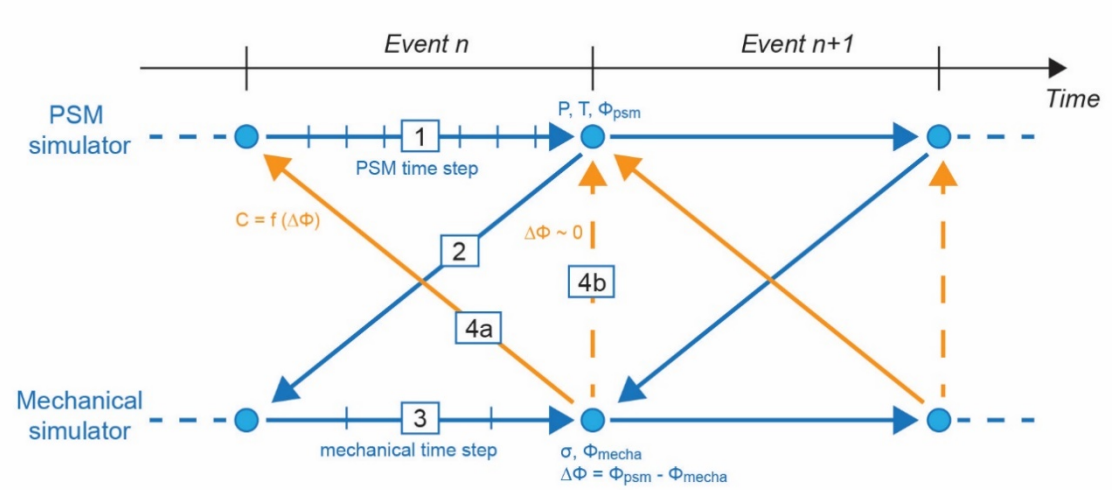

Figure 3 – Iterative coupling strategy implemented for the basin-scale simulations. In (1), PSM simulation is performed on event (n), which calculates outputs P (pressure), T (temperature), ϕ_{psm} (porosity from PSM). In (2), pressure field P is transferred to the mechanical simulator. In (3), mechanical simulation is performed on event (n), which calculates outputs σ (stresses) and ϕ_{mecha} (porosity from mechanical simulator). Porosity difference between the two codes is then evaluated ($\Delta\phi = \phi_{psm} - \phi_{mecha}$). If the porosity difference is higher than a chosen tolerance (4a), a corrective term C = f(Δϕ) is send to the PSM simulator (back to (1)). If not, the code proceeds to the next event (4b).

3.2 Data: Thermal state, compaction state and pore pressure in the Neuquén basin

Temperature distribution in the basin is retrieved from bottom hole temperature (BHT) available for six wells (Figure 4a), and the thermal evolution of the basin is analyzed from vitrinite reflectance data made available in seven wells (Figure 4b). Temperature sampling is localized at the top of the Tordillo Fm. Temperature values range from 117°C to 135°C depending on the wells (Figure 4a), and does not show a clear correlation with burial depth. It suggests that bottom heat flux may be spatially variable, probably because of heterogeneities in the lithospheric architecture and/or that temperature distribution is locally disturbed by magmatic activity(Spacapan et al, 2018; Sagripanti et al, 2020). Vitrinite reflectance is a thermal maturation indicator widely used to quantify the maturity of organic matters in sedimentary rocks (Tissot et al, 1987). In the Neuquén basin, these measurements show a substantial maturity variation at depth (Figure 4b), especially in the Vaca-Muerta and Quintuco Fms (these sedimentary formations are localized between 1500 and 2500m below the sea level). Maturity seems to increase toward the FTB along NE-SW axis, as W10 and W8 wells are clearly past the gas window in the Vaca-Muerta Fm, whereas the W6 and W1 wells still record low-grade immature rocks. This distribution complies with published maps of the Vaca-Muerta Fm thermal maturity at the scale of the whole Neuquén basin (Sylwan, 2014; Legarreta and Villar, 2015). While the maturity trend follows at first-order the basin morphology, it is not excluded that small maximum anomalies developed along major magmatic provinces, such as the one developed during the Cenozoic near the wells W1 to W7 (Figure 1a) (Sylwan, 2014; Spacapan et al, 2018).

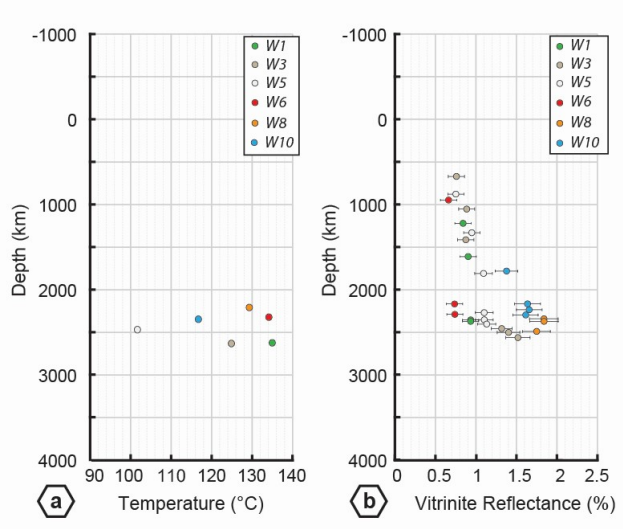

Figure 4: Thermal dataset available for this study. (a) Measured temperature for six wells (W10, W1, W8, W3, W5, W6) as function of true vertical depth. (b) Vitrinite reflectance data for six wells (W10, W1, W8, W3, W5, W6) as function of true vertical depth.

Figure 5 describes available information from ten wells which gives insight on pore pressure, and porosity evolution with depth. Most of these wells are located at the eastern side of the Chihuidos Anticline, with the exception of the W2 and W8 wells which are located at its northern closure and close to the fold hinge, respectively (Figure 1a). W10 and W9 wells are both located on the Chihuidos south-west limb, while the other wells are positioned farther from the fold influence.

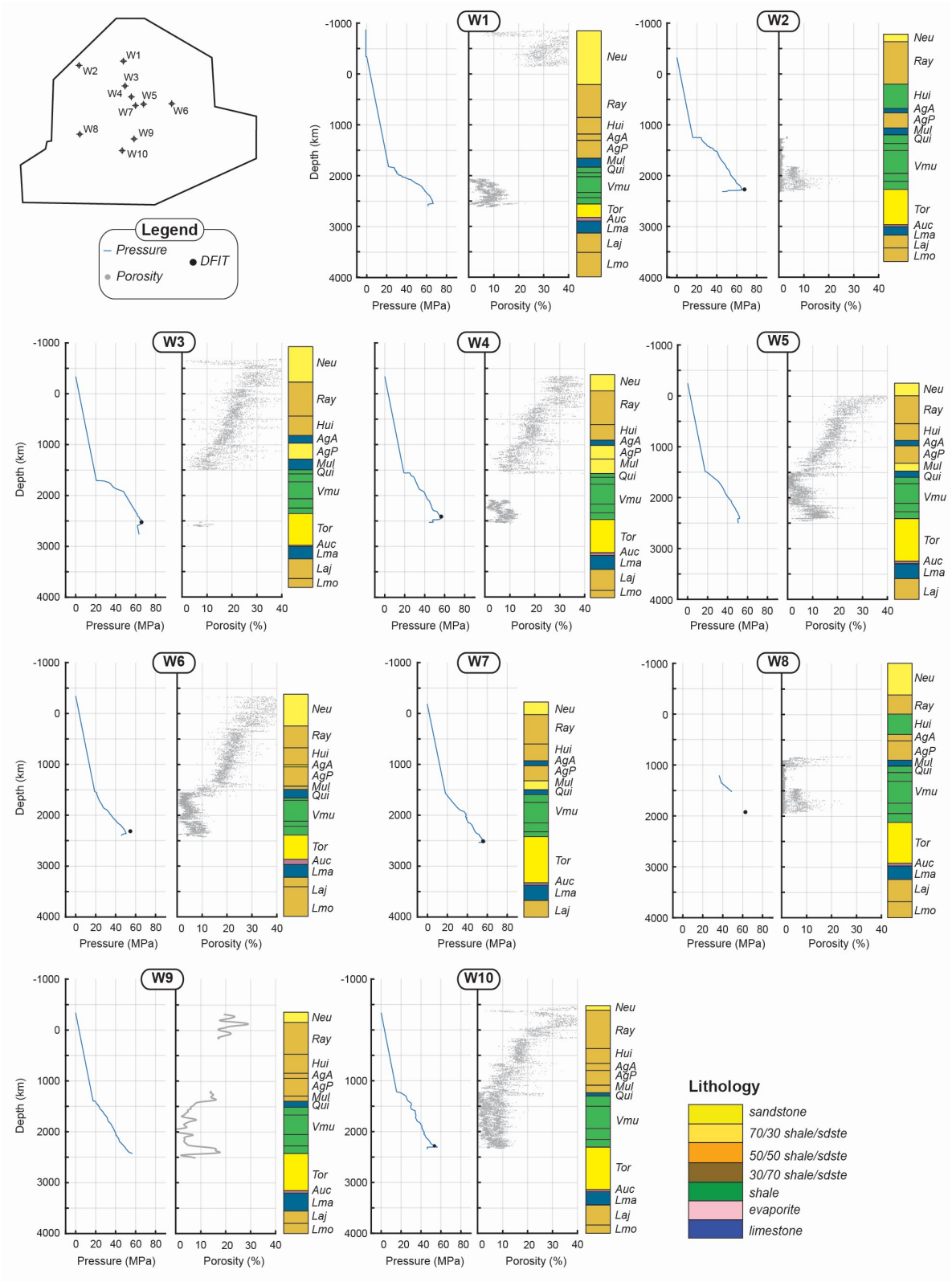

Figure 5: Pore pressure and porosity data. In the porosity plot, grey dots correspond to porosity measurements, and when existing, thick gray lines correspond to porosity computed from density measurements. For each well, the stratigraphy and lithology of the 3D model is reported. Lmo: Los

Molles Fm, Laj: Lajas Fm, Lma: La Manga Fm, Auc: Aucquilco Fm, Tor: Tordillo Fm, Vmu: Vaca-Muerta Fm, Qui: Quintuco Fm, Mul: Mulichinco Fm, AgP: Agrio Fm, Agua de Mula Member, AgA: Agrio Fm, Pilmatue Member, Hui: Huitrin Fm, Ray: Rayoso Fm, Neu: Neuquen Fm.

Porosity data on nine wells are used to describe the compaction state of the basin (Figure 5). Although dispersed, porosity values consistently show a pattern linearly decreasing with depth from ~30% at the surface to ~10% at the top of Quintuco Fm. In the Vaca Muerta Fm, the porosity ranges from 2 to 10%.

Pressure data derive from the processing of indirect measurement performed by Total. DFIT values were used to check the validity of these estimated pressure and are also included, when available. The pressure distribution in these wells shows hydrostatic pattern along the upper part of the sedimentary column (Figure 5), above the top of the Vaca-Muerta and Quintuco Fms. By contrast, an exceptionally high overpressure increasing downward is displayed within these formations. On several wells (W2, W4, W6, W9 and W10), a significant pressure peak is observed at the base of the Vaca-Muerta Fm, which tends to dissipate entering the Tordillo Fm (Figure 5).

4. Model set-up

4.1 Architecture of the 3D model

A 3D geological model populated with sedimentary facies (Figure 6) is built using 18 depth-converted seismic horizons, which covers the Chihuidos Anticline and the foreland. The model extends over 195 km west from the tectonic front, and covers 180 km from north to south (Figure 1a). It is mainly discretized using hexahedra cells with an horizontal size of 2x2 km (Figure 6a). The model is divided into 17 sedimentary layers with variable thicknesses, corresponding to the main stratigraphic formations above the Trias. It only comprises the post-rift and foreland section of the Neuquén basin, reaching a maximum depth of 8 km, while a uniform basement is considered below the Los Molles Fm.

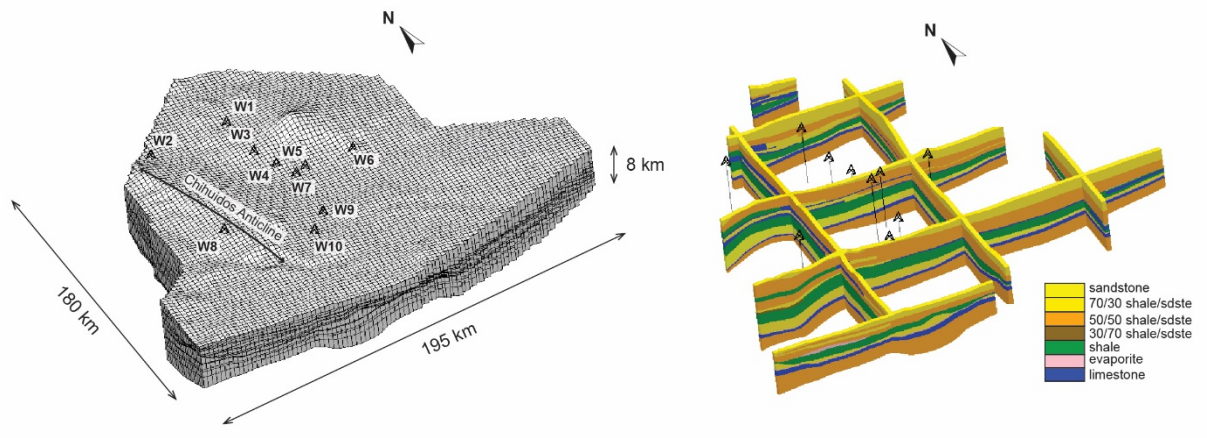

Figure 6: Architecture of the 3D geological model localized in Figure 1a. (a) Representation of the model mesh, with an X5 vertical exaggeration. (b) Several longitudinal and transversal sections of the model, colored by lithology. The lateral variation of thickness of the Vaca-Muerta shale is shown in green at the center of the stratigraphy, pinching out at the eastern and southern edge of the model.

As this part of the basin is not significantly affected by basin-scale faulting (Mosquera and Ramos, 2006), we consider it without fault to reduce the model complexity. It is motivated by the absence of faults with spatial extension and throw significantly higher than the cells size. Each sedimentary layer shows lateral thickness variations resulting from the shift of the depocenters during the sedimentation. At present-day, the basin architecture is mainly controlled by the Chihuidos structure, which appears as a large wavelength anticline that folds the whole model along its western boundary (Figure 6). The sedimentary layers are also significantly uplifted and pinched out toward the southwestern boundary of the model, corresponding to the transition to the Huincul Ridge domain (Mosquera and Ramos, 2006).

Lithological facies attribution have been assigned to the model cells according to paleogeographic maps from literature (Schwartz and Howell, 2005; Arregui et al, 2011; Spaletti et al, 2011; Leanza et al, 2011; Veiga et al, 2011; Zavala and Ponce, 2011; Garrido et al, 2011; Kietzmann et al, 2014, 2016). For the sake of simplification, lithologies have been merged into seven facies which we assumed hold similar petrophysical behavior (Figure 6b). In order to most accurately simulate the pressure increase in the Vaca-Muerta Quintuco Fm, the latter has been split into 5 sublayers, from top to bottom: the Quintuco facies, and four sub-units of the Vaca-Muerta facies. The thickness of these

sub-units significantly decreases from 1168m at the southern part of the Chihuidos Anticline to 100 m at southern and eastern border of the model (Figure 6).

4.2 Lithological facies properties

Thermal and mechanical properties, as well as compaction and permeability parameters have been assigned to the seven lithological facies. Values for these parameters may result from limited model calibration, with respect to standard values ranges found in Hantschel and Kauerauf (2009) and Turcotte and Schubert (2002). These values are given in Table 1 in the supplementary materials. Compaction parameters refer to the Schneider compaction law parameters (Schneider et al, 1996). Rock permeability is calculated using the Kozeny-Carman relation, except for the shale facies for which a specific porosity-permeability table of values has been considered. Parameters of the Kozeny-Carman relation assigned to each non-shale lithology are chosen so that drained conditions prevail in each lithological facies during burial. The shale facies permeability is slowly decreasing from 0.42 mDa at 60% of porosity to 1 µDa at 20% porosity, then suddenly decreases to strongly impermeable values at 10% porosity (1.5 nDa), after which it remains stable, reaching the constant value of 1 nDa at 5% porosity. This evolution is the result of model calibration, and is thought to better describe the diagenesis of the Vaca-Muerta Fm shales. Given the fact that, in the coupled model, elastic properties evolve in function of porosity, the initial values of Young modulus (E_0) and and Poisson's ratio (ν_0) are prescribed for each lithology so that the targeted E and ν at the end of the simulation are coherent with values of rocks lithologies at their burial level at present-day (Zoback, 2010).

4.3 Reconstruction of paleogeometries from backstripping

Given the low structural deformation, forward simulation is run with paleogeometries provided by backstripping. The subsidence history in the model extent is well represented by the burial curve calculated at the location of the W10 well (Figure 7). The basin undergoes three stages of burial and exhumation: a sedimentation stage followed by a hiatus period and, lastly, exhumation. The latter is characterized by significant uplift and erosion partly associated with the folding of the Chihuidos Anticline.

Various sedimentation rates are observed from the deposition of the Los Molles Fm (Lower Jurassic) to the deposition of the now eroded Malargue Fm (Paleocene). A deeper basin topography at the

western side of the model is prescribed during the post-rift sedimentation, with water depth reaching 500m. From the deposition of the Rayoso Fm, paleobathymetry is fixed to zero in the entire model. From the Paleocene to the Middle Miocene, a 46 My hiatus is prescribed, to model the tectonic quiescence and low sedimentation rates observed in the basin during the Eocene and Oligocene (Zamora Valcarce et al, 2009). Lacking data on the Miocene sediment distribution and considering its low thickness, we merge it with the Paleocene sedimentation. Finally, exhumation (defined as simultaneous uplift and erosion) occurs linearly since the Late Miocene until present, starting 10 My ago. The eroded thickness of the Malargue and Neuquén Fm deduced from 1D calibration in wells from both sonic log and vitrinite dataset is consistent with the published results of Zamora-Valcarce et al (2009) at the hinge of the Chihuidos Anticline. Erosion ranges from 500m to 2080m, with an increasing trend towards the southwest part of the model. The hinge of the Chihuidos Anticline records the most important values, which follows the NW-SE axis of the fold. Simultaneously with erosion, the sedimentary layers are uplifted to their current topography, while the Chihuidos Anticline development leads to the folding of the sedimentary layers.

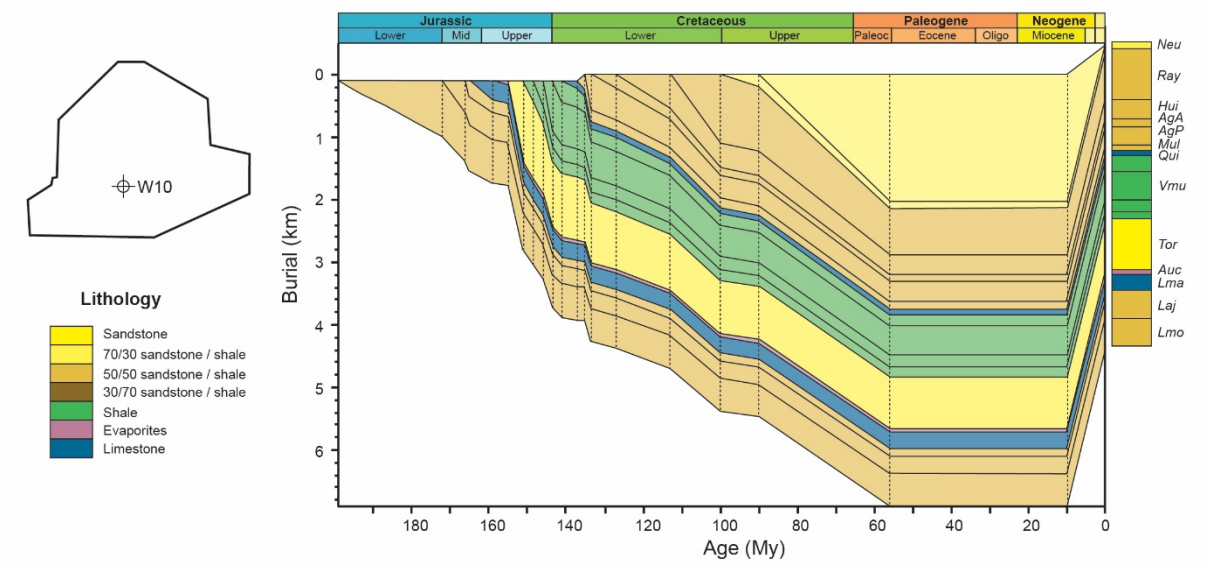

Figure 7: Burial curve displaying the lithology and burial evolution of each sedimentary formation during the Mesozoic and Cenozoic at the W10 position.

4.4 Mechanical properties and boundary conditions adopted in the PSM and coupled simulation

No-fluid flow conditions are prescribed on the lateral and bottom surfaces of the model, while the piezometric surface is set to the surface topography. Similarly, no-flux thermal conditions are imposed on the lateral surfaces, and the top surface temperature is prescribed. Basal heat flow is calculated using a lithospheric model defined at the base of the sedimentary model. It is composed of three main layers : the upper crust, the lower crust and the upper mantle. The Moho depth is defined referring to Rojas-Vera et al (2014) while the thickness of the upper mantle is initialized from the ICONS Atlas (Heine, 2007). Crustal thickness is divided evenly between the upper and lower crust. It varies from 32 km to 37 km, with minimum values at the eastern side of the Chihuidos Anticline (Rojas Vera et al, 2014), while the mantle thickens northward to from 75 km to 85 km.Temperature at the base of the lithosphere is fixed at 1333°C (e.g. Hantschel et al, 2009).

In the coupled simulation, tectonic loading is applied along the E-W direction starting from the Late Miocene in the lateral surface of the model, simultaneously to model exhumation. As we assume it is the main event deforming the foreland (Zamora-Valcarce et al, 2009; Rojas Vera et al, 2015), only this shortening period is considered in the model of the tectonic scenario. The shortening direction is inferred from the broadly N-S fold axis in the adjacent FTB (Figure 1a), from shortening vectors given by GPS measurements (Klotz et al, 1999) and from the first-order E-W direction of the maximum horizontal stress measured in wells (Guzman et al, 2007). Shortening is applied in two sequences during exhumation. Shortening rates and timing are the parameters mainly used to calibrate model pressure and porosity:

- From 10My to 8My, 4% of shortening is prescribed to model the main Andean deformation phase during the Miocene.
- From 8My to present-day, 2% of shortening is prescribed, accordingly with the more limited deformations observed in the Neuquén basin during the Plio-Quaternary.

5. Results

The simulations have been performed with the coupled workflow, as well as with the PSM code alone for comparison. In both cases the geological scenario and material properties are identical. Thermal results did not show any significant difference between the PSM and the coupled simulation. Calculated vitrinite reflectance along the five wells displaying thermal data shows a very good fit with the measurements with a maximum difference of 0.2 %, while the westward increase in thermal maturity from gas window to immature rocks, observed in the data, is also respected (Figure 8). Similarly, simulated present-day temperature shows less than 5°C difference with the bottom-well temperature data. These two results ensure the consistency of our thermal and structural modelling. While thermal predictions are similar with or without tectonic loading, major differences could be observed when comparing pressure predictions. The latter are detailed in the following section.

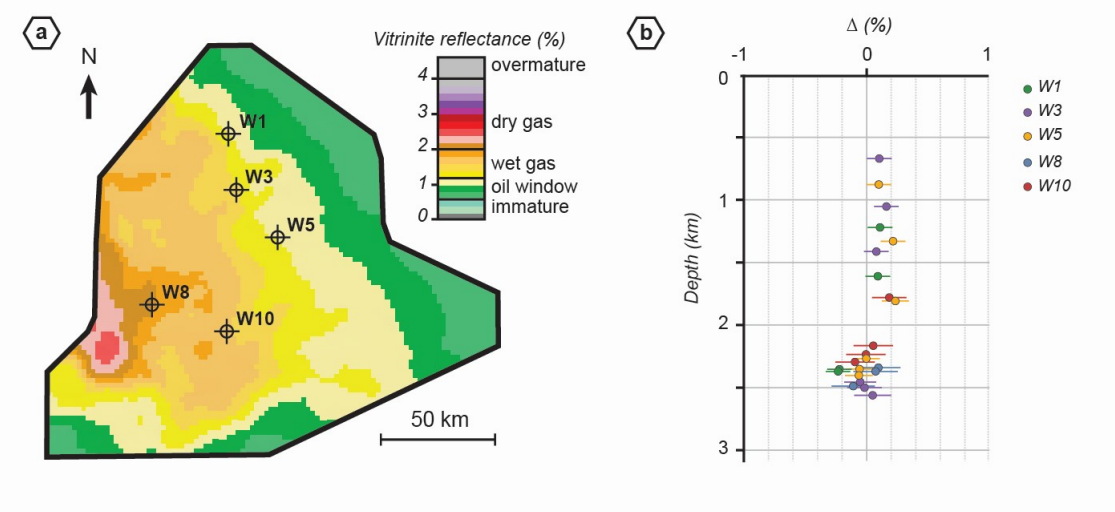

Figure 8 – Vitrinite reflectance modelling results compared to the available data. (a) Distribution of the vitrinite reflectance in the lower layer of the Vaca-Muerta. (b) Plot of the difference between the simulated vitrinite and the measured data vs. depth, for each well.

5.1 Comparison of present-day pore pressure prediction in the Neuquén basin using the PSM and the coupled simulation

Present-day overpressure distribution is detailed for a horizon at the base of the Vaca-Muerta Fm and in a section crosscutting the Chihuidos Anticline, for both the PSM (Figure 9a) and the coupled simulation (Figure 9b). The PSM simulation shows a quasi-hydrostatic pressure field in almost all the basin, with a maximum overpressure close to 3 MPa observed at the base of the Vaca-Muerta Fm.

This overpressure is localized at the eastern side of the Chihuidos anticline, and extends below the Vaca-Muerta seal. It results from the low permeability of this formation and transfer of fluids during exhumation. The most exhumed regions of the model (the hinge of the Chihuidos Anticline, for instance) display slight underpressure, which results from the exhumation of the model above sea level.

Contrary to the PSM results, significant overpressure is generated in the coupled model within and below the Vaca-Muerta Fm (Figure 9b). At the base of the Vaca-Muerta Fm where highest pore pressure is recorded, overpressure shows a very heterogeneous distribution. It ranges from 30 MPa where most burial is achieved, to hydrostatic in the eastern and southern part where seal permeability remains large enough to dissipate the pressure. The section across the Chihuidos Anticline clearly shows the division of the model into two distinct compartments, separated by the Vaca-Muerta Fm. The upper compartment shows entirely drained conditions with hydrostatic pressure. The Vaca-Muerta Fm acts as an effective seal, maintaining the elevated pore pressure caused by tectonic loading in the lower compartment. This behavior is amplified by the impervious conditions at the model boundaries, which prevent lateral fluids migration away from the FTB. The NW-SE overpressure drop at the hinge of the Chihuidos Anticline is also observed within and below the Vaca-Muerta Fm, coinciding with the distribution of the underpressure observed in the PSM results (Figure 9a).

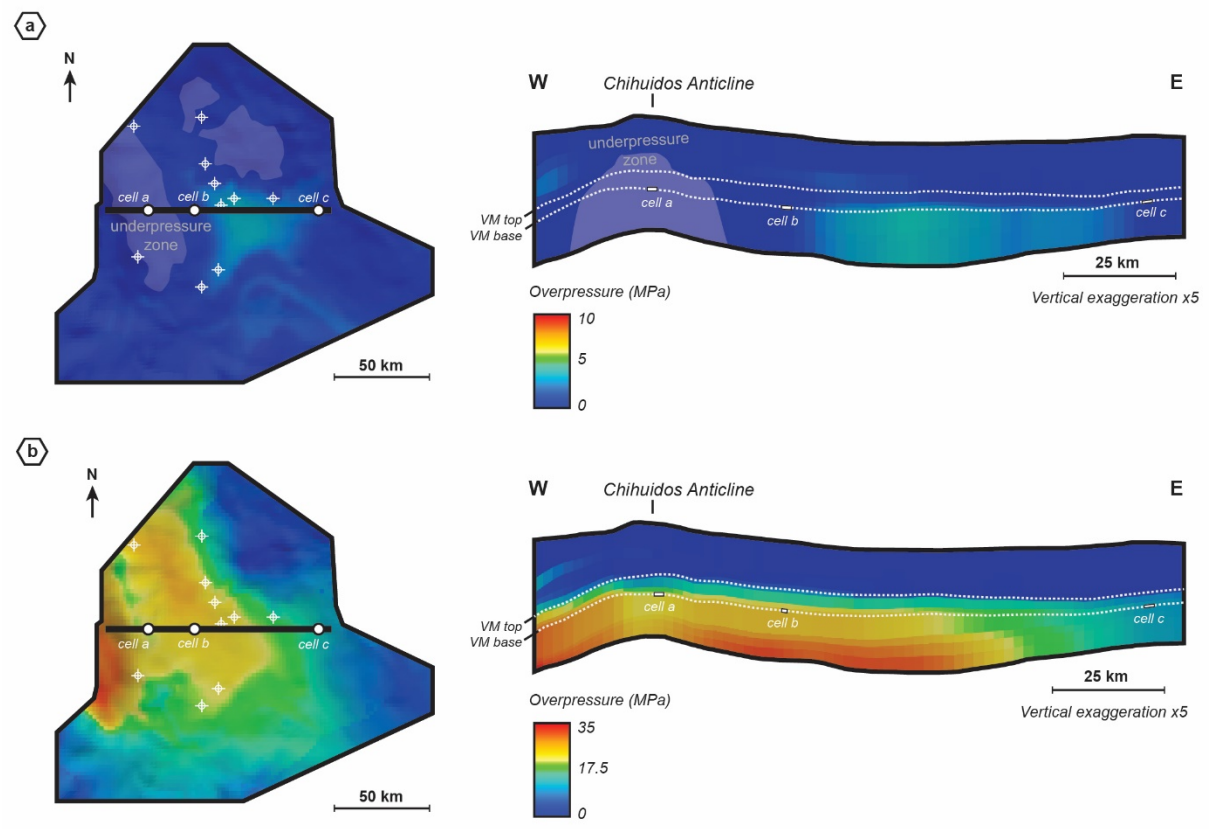

Figure 9 – Present-day overpressure distribution resulting from the PSM and the coupled simulation, in the base layer of the Vaca-Muerta Fm and in a section crossing the Chihuidos Anticline. Well position is reported. Cells a, b and c highlight the position of the cells displayed in Figure 11. (a) Result of the PSM. (b) Result of the coupled simulation.

Pore pressure and porosity distribution vs. depth plots resulting from the coupled simulation are shown for each well in Figure 10 and compared to the available data. PSM results are not presented, as they roughly align with the hydrostatic pressure. Calculated porosity decreases with depth in accordance with the data. In the upper compartment, above the Vaca-Muerta and Quintuco Fms, simulated pore pressure and data strictly follow a hydrostatic profile, except for the W8 and W2, along which the Huitrin shales show a slight overpressure. It should be noted that for several wells, including W1, W2 and W3, calculated hydrostatic pressure is larger than the data, because of piezometric conditions in these wells which are not considered in our model. Simulated overpressure in the Vaca-Muerta Fm consistently matches the well data, with a maximum relative gap below 10% for the the wells W3 to W10. The two northernmost wells display underestimated overpressure, with pressure difference up to 10 MPa in the W1 well. No pressure data are available in the lower compartment,

except at the top of the Tordillo Fm where a sudden drop of overpressure is observed, contrary to what is obtain in the simulations where it still increases. The no-flow condition prescribed at the model boundaries in the absence of constraining data explain this deviation. It inhibits fluid expulsion from the deeper reservoirs to the foreland despite the drained conditions, preventing an overpressure dissipation mechanism classically observed in foreland basins (Roure et al, 2005).

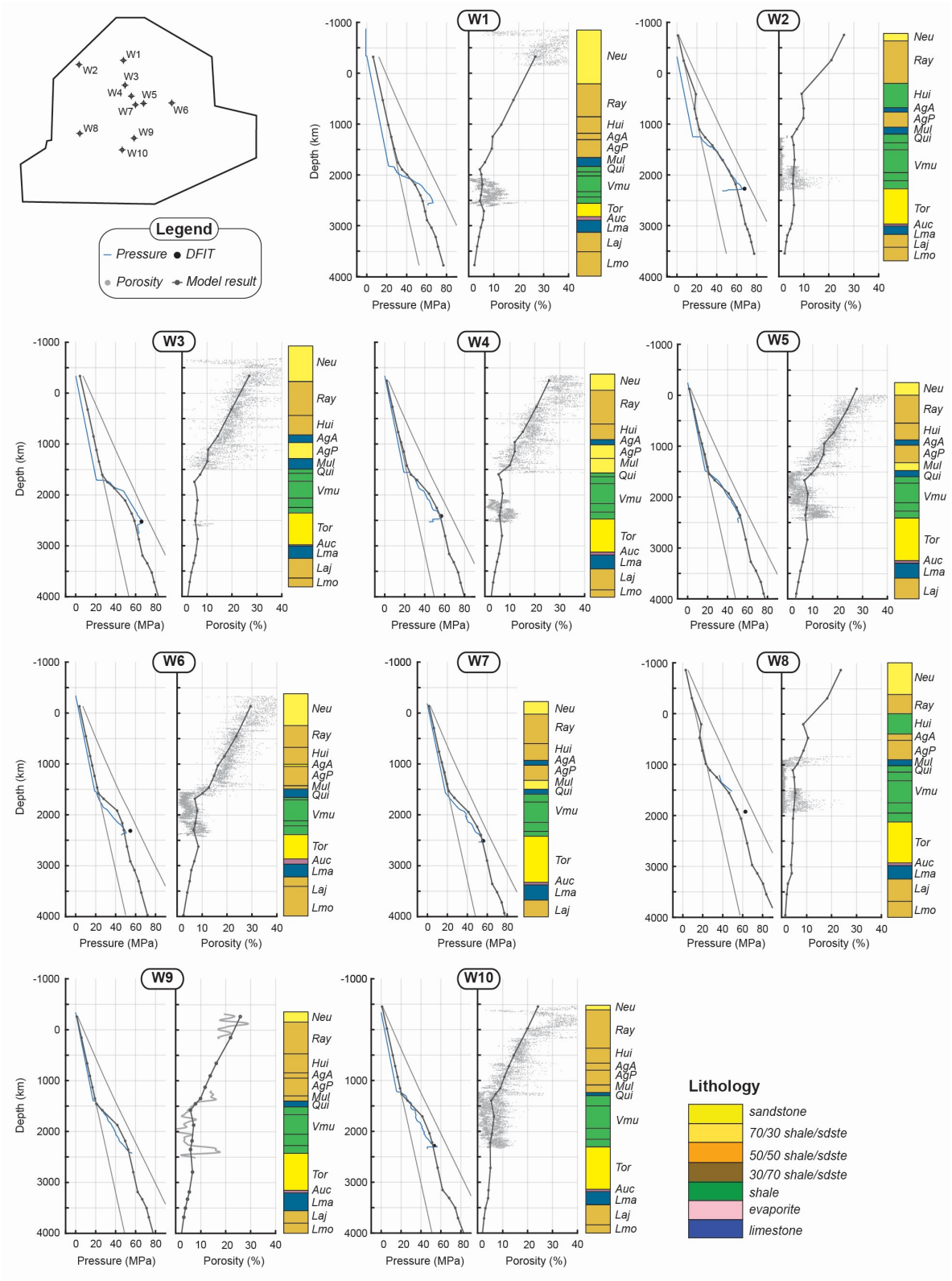

Figure 10 – Pore pressure and porosity results of the geomechanical coupling compared with the available data. In the pressure and porosity plots, bold gray lines correspond to the pressure given by the simulation, while the thin grey lines in the pressure plot correspond to the computed

hydrostatic and lithostatic pressure.

5.2 Comparison of the pore pressure evolution in the Neuquén basin within the Vaca-Muerta Fm using the PSM and the coupled simulation

Pore pressure evolution at the base of the Vaca-Muerta Fm in both the PSM and coupled simulations are reported in Figure 11 for three cells. Each cell has a different location with respect to the Chihuidos Anticline (Figure 9): Cell (a) is at the hinge of the Chihuidos Anticline, cell (b) is in the eastern limb of the fold, close to the area of maximum observed pressure and cell (c) is in the eastern part of the model.

Coupled simulation and PSM show the same trend of pore pressure evolution during the sedimentation phase (Upper Jurassic to Paleocene). Pore pressure strongly increases from the beginning of the sedimentation until the deposition of the Agrio Fm (Lower Cretaceous), consistently with the high sedimentation rates recorded during this period. Overpressure rises with a peak of few MPa at the base of the Vaca-Muerta Fm during the Agrio Fm deposition (Lower Cretaceous), because of vertical disequilibrium compaction. The Neuquén-Malargue Fm deposition (Upper Cretaceous-Paleocene) shows a similar rise, notably visible in cell (a) and (b). However, this overpressure is completely dissipated during the Paleogene hiatus, making the basin fully drained before the Miocene to present-day exhumation and shortening.

During the exhumation phase, in the PSM, erosion prevents the generation of overpressure, except in cell (b) where a 2 MPa overpressure is creating by pressure fluid transfer, as already described in section 5.1. The model exhumation leads to significantly decrease the pore pressure, the amplitude of which is controlled by the eroded thickness. In the hinge of the Chihuidos Anticline, exhumation even leads to negative overpressure values showing the physical limits of our model at very low pore pressure.

The coupled simulation shows a different pressure evolution during this last phase because tectonic loading is now taken into account. For the three reference cells, the first shortening phase starts with a sudden pressure increase exceeding 40 MPa for cell (a) and (b) in response to the prescribed lateral loading, shortly followed by a pressure stabilization or even decrease. During the second shortening phase, pressure first accelerates and than tends to rise again after 2 to 3 My until it reaches its

present-day values. In the coupled simulation, the combination of erosion, uplift and shortening triggers multiple interacting geomechanic and hydrodynamic phenomena, making the interpretation of the multi-physics coupling difficult to decipher. Still, three phenomena predominate, each having contrasting effects:

- Erosion decreases the vertical load (i.e. lithostatic stress), leading to pressure decrease.
- Uplift modifies the air-water surface, which in turn modifies the model hydrodynamism, leading fluids to flow outward the most uplifted regions.
- Shortening tends to compact the rock materials, leading in return to strong overpressure increase where low permeability keeps the fluid from escaping rock porosity.

The evolution of pore pressure during shortening suggests that tectonic loading predominates in the early step of the exhumation, leading to overpressure increase. In cell (c), overpressure is limited because of the small thickness of the seal formed by the Vaca-Muerta Fm. However, at some point during the first shortening phase, pressure decreases due to erosion and uplift seems to take over as the primary mechanism although tectonic loading continues. Overpressure stabilizes or even decreases for the cells (a) and (b), both of which being characterized by higher erosion rates than in cell (c). During the second shortening phase, pressure rebalancing between the different layers of the Vaca-Muerta Fm makes overpressure to increase again.

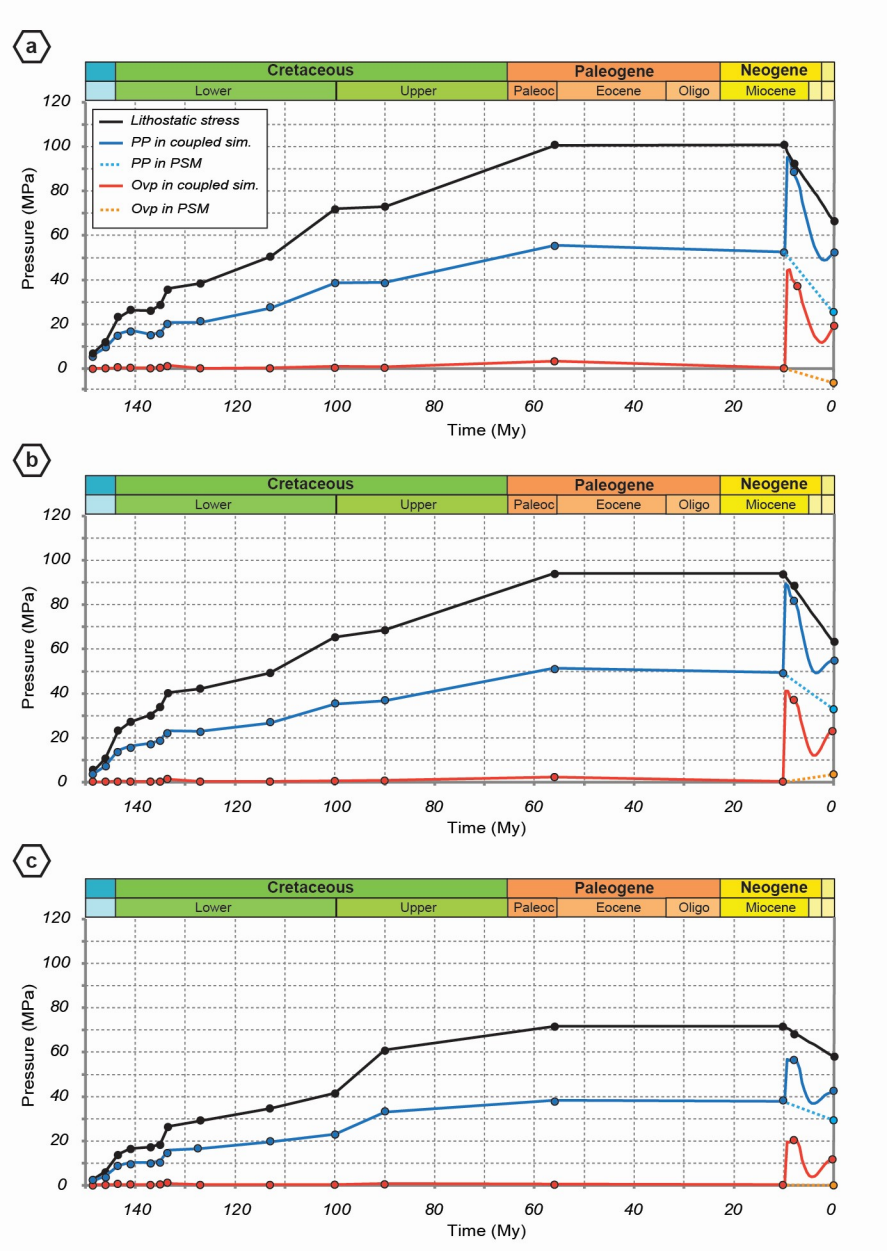

Figure 11 – Evolution of the pore pressure, overpressure and lithostatic stress over time for three cells of the base layer of the Vaca-Muerta Fm. Dots indicate the end of simulation time-steps. During the exhumation, these dots represent the end of the two successive phases. Position of the cells are given in Figure 9. (a) Evolution of the hinge of the Chihuidos Anticline. (b) Evolution of the eastern limb of the Chihuidos Anticline. (c) Evolution of the eastern region of the model.

5.3 Fracturing assessment of the Vaca-Muerta Fm seal rocks.

Prediction of natural fracturing in classic PSM is quite limited because the full 3D stress tensor remains unknown. Fractures are assumed tensile and are supposed to develop when pore pressure exceeds an unknown minimum horizontal stress, which is defined as a given fraction of the vertical lithostatic stress (e.g. Tuncay and Ortoleva, 2004). No fracture is likely to develop in the Neuquén basin according to this hypothesis, because of the large difference between pore pressure and lithostatic stress during the basin evolution (Figure 11), which is contradictory with the numerous fracture observations in the basin (Branellec et al, 2015; Ukar et al, 2017; Larmier, 2020).

By contrast, the 3D geomechanical approach calculates the minimum horizontal stress instead of relying on a first-order approximation for its value. In addition, this approach makes it possible to analyse the risk of shear fracturing. With the constitutive model used in our approach, a preliminary criterion to predict the possibility of shear-induced fractures is given by the change in the plastic regime from ductile failure at the right side (compaction) to brittle failure at the left side (dilation) of the CamClay yield surface (Bemer et al, 2004), the two domains being separated by the Critical State Line (CSL) (Figure 12b). We also use the equivalent Von Mises strain (a measure of distortion) to quantify the amount of shear deformation that occurs in the dilatant side of the plastic model. In the following discussion, this indicator of shear-induced dilation will be referred to as fracturing, implying that fracturing in our model always involves a shear component. This is a simplification aiming at capturing the beginning of fracturing in order to investigate the behaviour of the coupled model only. For this reason, the rock permeability is not changed even if fracturing is detected.

A 3D view and two cross-sections shown in Figure 12a show the present-day distribution of fracturing at the base of the Vaca-Muerta Fm. Von Mises strain principally increases in the vicinity of the Chihuidos Anticline, and only in overpressured sedimentary layers (i.e. in the Vaca-Muerta Fm and below). Shear fracturing develops in a large zone extending over most of the north-western quadrant of the model. The Von Mises strain reaches its maximum value at the edge of the fold, especially in the steeper western limb, while the fold hinge displays significant but lower values, in accordance with the overpressure distribution observed in Figure 9b. This is a consequence of the high overburden on these layers, so that a significant fluid overpressure build-up is necessary in order to trigger the shear-induced fracturing mechanism.

The stress path of a cell at the base of the Vaca-Muerta Fm, in the southern part of the fractured zone, is drawn in the (*p'*;*q*) diagram (Figure 12b), with p' the mean effective stress and q the equivalent deviatoric stress. Stress paths in (*p'*;*q*) diagram grants key information on the deformation history and rock geomechanical behavior (Wood, 1990). From its deposition at 151 My to the onset of tectonic at 10 My, the stress path follows a linear trend corresponding to cell burial. When the first shortening phase starts, it abruptly changes direction and briefly crosses the CSL. Then, the stress path returns to the compaction domain until the end of this phase. It must be noted that the stress path crosses the CSL only once, meaning that the fractured zone entirely developed during this first shortening period. We can explain the fracture zone distribution by the variable thickness of the Vaca-Muerta Fm and the variable rates of tectonic loading, uplift and erosion in each cell, which lead to different stress paths. In the second tectonic phase, the prescribed shortening rate is slower, allowing for fluids to be expulsed while rock compaction continues, causing the increase of the plastic yield surface size (Figure 12b). This initially make the stress path to follow again the trend of the burial period. At some point, the overpressure increases again, and the stress path starts to move back toward the CSL again.

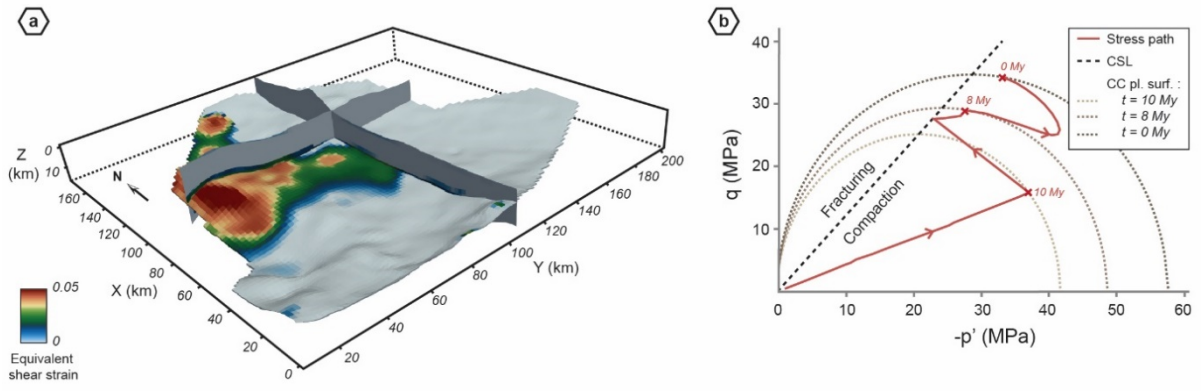

Figure 12 – Natural fracturing of the Vaca-Muerta Fm in the coupled simulation. (a) 3D view of the model showing the distribution of the cumulated von Mises strain, or fracturing. Vertical exaggeration is set to x5. (b) Stress path of a cell from the base layer of the Vaca-Muerta Fm, in a (p';q) diagram. The CamClay yield surfaces are computed for three key events of the simulation.

6. Discussion

6.1 Overpressure development: PSM vs. coupled simulation

The comparison of the PSM and the coupled simulation results points out that disequilibrium compaction from burial is not able to generate overpressure in the Vaca-Muerta Fm, whereas additional loading from tectonic can be sufficient to generate the observed overpressure. In addition, predicted spatial distribution of overpressurized zones are different (Figure 9).

The different evolution observed during the exhumation period illustrates their respective behaviour regarding the Miocene-recent phase:

- In the PSM, in the absence of sedimentation, pore pressure can only decrease linearly according to erosion. The model hydrodynamism does not modify the pressure distribution beyond few MPa during this period. Because the model exhumation initiates in drained conditions (Figure 11), it is impossible to develop overpressure with the chosen simulation parameters.

- In the coupled simulation, the evolution is strongly non-linear and controlled by 3 parameters (tectonic loading, uplift and erosion). Tectonic loading is able to generate and maintain significant overpressure, assuming the shortening is sustained during all the exhumation period, otherwise pore pressure rapidly dissipates.

The difference in spatial distribution and the non-linear evolution of the overpressure in the coupled simulation emphasizes that tectonic loading does not constitute a pressure scaling factor that is uniformely applied in all the cells' model.

6.2 Limitation of the model calibration with regard to overpressure mechanisms unrelated to stress

PSM studies, coupled or not, use a necessary step of calibration to match the model with observable variables (Hantschel and Kauerauf, 2009). As the main objective of this work is to analyze the impact of tectonic shortening on PSM, we decided to use shortening rates and their respective timing as the main calibration parameters of the coupled simulation. Therefore, their values are a direct result of the porosity and pressure calibration. This assumption should be discussed in light of other prescribed parameters or overpressure mechanisms not taken into account in this study. As such, these results

should be merely taken as a possible scenario among others, demonstrating that in an extreme case, Miocene to recent tectonic loading is the main contributor of the Neuquén basin overpressure.

With regards to the Neuquén basin, one of the limitation is given by the absence of fluid expansion mechanisms other than the aquathermal expansion (Swarbrick et al, 2001). Notably, the contribution of the kerogen transformation and gas generation on the overpressure development is disregarded, while it has been described as an important mechanism for overpressure generation (Osborne and Swarbrick, 1997; Tingay et al, 2013), and particularly for the Vaca-Muerta Fm fracturing (Rodrigues et al, 2009; Zanella et al, 2015). Several studies quantify how much gas generation can lead to overpressure development (Hansom and Lee, 2005; Guo et al, 2011; Luo et al, 2016), and, in this regard, the PSM thermal modelling illustrates that the Vaca-Muerta source-rock passed through the gas window in most of the model (Figure 8). In our model, PSM simulation shows that fluid supply from hydrocarbon generation in the Vaca-Muerta Fm begins at the transition from Lower to Upper Cretaceous, as measured by Rodrigues et al (2009), Ukar et al (2017) and Weger et al (2019).

Consequently, hydrocarbon generation should form an additional and continuous contribution in the Vaca-Muerta overpressure through the Miocene-recent period, in addition to tectonic loading, which in turn should decrease the shortening value identified by model calibration. It remains to be seen if, in a scenario where extreme volumes of hydrocarbon are generated, present-day overpressure could be reached without tectonic loading. Specifically in our model, even if a total transformation ratio of the kerogen is reached and a high volume of hydrocarbon fluid is generated, this volume would be distributed over all the Cretaceous-recent period, reducing its impact on the overpressure. Consequently, with the high permeability prescribed for the Vaca Muerta Fm, it is more likely that the continuous erosion and uplift since the Miocene would still reduce too much the pressure to calibrate the wells data, as seen in the case of the PSM simulation.

6.3 Insight from coupled simulation into the Vaca-Muerta Fm fractures development

The Vaca-Muerta Fm contains widespread, thick bed-parallel veins that have been widely described (Rodrigues et al, 2009; Cobbold et al, 2013; Zanella et al, 2015; Ukar et al, 2017; Weger et al, 2019; Ravier et al, 2020; Larmier, 2020; Zanella et al, 2020). Classical observation of hydrocarbon inclusions in these bed-parallel veins infers that overpressure during oil and gas generation is an

important mechanism for their formation (Rodrigues et al, 2009), but horizontal shortening is often invoked as another important mechanism (Lash and Engelder, 2005; Cobbold and Rodrigues, 2007; Rodrigues et al, 2009; Zanella et al, 2015; Ukar et al, 2017; Larmier, 2020; Zanella et al, 2020). In addition, a more classical fracture network is observed, characterized by different sets of joints of various orientation and various scale reflecting the stress evolution in the basin (Sagasti et al, 2014; Branellec et al, 2015).

The numerical simulation suggests that overpressure resulting from vertical disequilibrium compaction is not sufficient to fracture the Vaca-Muerta Fm. Therefore, models for the bed-parallel veins opening cannot rely solely upon vertical mechanical compaction. It must take another mechanisms into account, for instance tectonic compaction (this study) and/or kerogen to gas transformation (Rodrigues et al, 2009; Zanella et al, 2020). This study shows that a single Late Miocene tectonic event is sufficient to promote shear fracturing in the Vaca-Muerta Fm, in a compressional stress regime, if a sufficient deformation rate occurs. This fracturing event occurs even if pore pressure does not exceed the lithostatic stress. This implies that the fracturing of the Vaca-Muerta Fm only occurred when the basin was subjected to tectonic loading, whether it was since the Late Miocene, as proposed here, or possibly during the Upper Cretaceous-Paleogene shortening phase. It confirms the observations of Rodrigues et al (2009), Ukar et al (2017) and Zanella et al (2020) on the role of horizontal shortening in bed-parallel veins growth. As discussed in the previous chapter, it does not preclude that other parameters helped to fracture the Vaca-Muerta Fm, such as hydrocarbon generation for instance (Zanella et al, 2020).

In addition, the model indicates that fracture development in the Vaca-Muerta seems favoured by the Chihuidos anticlinal growth, when the coupled effects of erosion, uplift and tectonic loading occurs. Large-scale folding does not seem to be a necessary parameter for fracturing, and in fact, observation of fractures in the Vaca-Muerta Fm are widely distributed over the Neuquén basin (Larmier, 2020), even distant of major structural folds. That being said, the model suggests that, fracturing in the Neuquén basin isconsiderably facilitated by the coeval mechanisms exhumating the sedimentary rocks, at least during the Miocene deformation phase.

6.4 Miocene LPS deformation as a driving mechanism for the overpressure development in the Neuquén basin

We propose that the present-day fluids overpressure observed in the Neuquén basin developed simultaneously to the Miocene to present-day Andean deformation, existing at the scale of the Central Andes orogen (Horton, 2018). Pore-scale deformation (or LPS deformation) has already been identified as an important feature of the Neuquén basin (Branellec et al, 2015). We suggest that these Late Miocene to recent LPS deformations, here represented as lateral compaction, are likely to contribute significantly to the overpressure, as proposed in other settings by Couzens Schultz and Abdel (2014) and Obradors-Prats et al (2017). The model shows that this overpressure developed as a sudden pulse, promptly leading to rock fracturing. It suggests that the tectonic loading must be thoroughly sustained to maintain this considerable overpressure, even when seal permeability increase by fracturing is not taken into account, like in our models. Any decrease of the shortening rates leads to rapid pressure decrease. It underlines that the present-day tectonic stresses, while characterized by rates lower than those of the Late Miocene, are key to preserve overpressure in the Neuquén basin.

In this work, a single and continuous Miocene shortening is selected to develop overpressure, and this hypothesis can be more thoroughly discussed. Firstly, while a range of values for the timing and duration of these sub-events can be estimated by geological observations (Zamora-Valcarce et al, 2006; Zamora-Valcarce et al, 2009), there is no clear objective criterion to validate the shortening rates resulting from the model calibration. These rates are notably difficult to measure, and can range from 5% to 30% depending on the geological settings (see the different examples of Mitra, 1994; Sans et al, 2003; Koyi et al, 2004; Butler and Paton, 2010; Lathrop and Burberry, 2015). In the Neuquén foreland, shortening values from structural restoration remains lower than few kilometers, accommodated by several crustal-scale structures such as the Chihuidos Anticline (Zapata and Folguera, 2005; Messager et al, 2010; Rojas Vera et al, 2015). The fact that the last phase of shortening mainly deforms Mesozoic sedimentary rocks that was already deeptly buried and compacted suggests that the remaining potential for further compaction is limited (Butler and Paton, 2010). It favors LPS values that do not exceed few % over the model extent. A quick calculation can be made in light of the GPS displacements rates reported by Klotz et al (1999). Four stations indicates about 2mm/y of E-W shortening between the inner FTB and the eastern limit of our model. We can assume that this rate remained stable during the last 10 My, which is a very strong hypothesis regarding the Neuquén basin geological history, because the current shortening is probably lower than

those of the Late Miocene (Zamora Valcarce et al, 2006). It indicates that about 8% of shortening must be accounted for in the 195km of the model. This value far exceeds the one used in the simulation (4% for the Miocene tectonic phase, 2% until present-day), and the values calculated by structural restoration (Rojas Vera et al, 2015; Lebinson et al, 2018; Sánchez et al, 2018). It would also results in unreasonable pore pressure values and compaction level in the coupled simulation. However, this value encompasses shortening processes at different scales, including both faulting/folding and LPS deformation, within the inner FTB and the foreland. It can therefore be considered as a rough order of magnitude, making the value of the shortening used in the simulation conceivable.

Secondly, with regards to LPS deformation, special attention must be paid to the Upper Cretaceous tectonic shortening phase. In this work, we assume that tectonic loading does not affect the foreland during this major tectonic event, even if it considerably deformed the Agrio and Chos Malal FTB (Zapata and Folguera, 2005; Zamora Valcarce et al, 2006). This assumption can be challenged, since the Upper Cretaceous tectonic front is supposed to be localized less than 20 km west of the model (Rojas Vera et al, 2015). In addition, the bed-parallel veins in the Vaca-Muerta Fm have already been dated to the Upper Cretaceous, not only in the internal part of the FTB, but also near the current tectonic front (Rodrigues et al, 2009; Ukar et al, 2017; Weger et al, 2019). In the present work, overpressure development resulting from Late-Cretaceous tectonic loading would be too difficult to constrain without further data on the paleo-pressure history. It is assumed that the Late-Cretaceous overpressure is very likely to be completely dissipated throughout the Paleogene-Neogene sedimentation hiatus, with regards to the PSM and coupled pressure evolution described in section 5. Therefore, we assume that the present-day pore pressure would not be significantly modified in the model if this shortening event were taken into account. Nonetheless, it is likely that such event would lead to seal fracturing, similarly as during the Miocene tectonic phase, which could explain the Upper Cretaceous ages of the bed-parallel veins. It could also potentially modify the Miocene fracturing pattern, assuming the likeliness of fractures reactivation.

7. Conclusions

This study shows that coupling a PSM with a geomechanical code makes it possible to assess the role of the Andean tectonic on the poro-mechanical evolution of the Neuquén basin. The Neuquén

basin underwent several shortening phases since the Upper Cretaceous, resulting from the Andean orogeny. Besides, the Vaca Muerta Fm displays exceptionally high fluid overpressure around the crustal-scale Chihuidos Anticline showing that the Vaca-Muerta Fm forms an efficient seal. Here we show that these overpressure could have been enhanced by the Andean tectonic shortening.

The coupled simulation account for a 3D poro-mechanical framework by the means of a constitutive law adapted from the modified CamClay model, enabling to model the contribution of lateral deformations from tectonic loading on the overall porosity and pressure and to calculate a shear fracturing criterion.

By means of this coupling, we calibrated the Neuquén basin pore pressure and porosity using tectonic phases since the Late Miocene, representing the last Andean deformations in the basin: (1) 4% of shortening from 10 My to 8 My and (2) 2% from 8 My to the present-day. This calibration cannot be achieved using the classic 1D vertical compaction model embedded in PSM. However, it is possible that the shortening values resulting from our modelling remain too high, because currently we lack the possibility to simulate the contribution of hydrocarbon generation in the overpressure. It advocates for further numerical studies fully integrating tectonic and hydrocarbon generation to discuss this particular point in the Neuquén basin. Still, we show that Andean Miocene to recent tectonic could explain most of the overpressure observed in the Vaca-Muerta Fm, even without considering other classical overpressure mechanisms. Other pulses of fluid overpressure in the sedimentary formation may have occurred during older deformation phases, resulting from the Upper Cretaceous FTB development for instance. This work also suggests that the Vaca-Muerta Fm fracturing, including the bed-parallel veins, is very likely to occur during one of these Andean deformation phases, helped by fluid overpressure and, to some extent, by rock exhumation.

This study can be used as an example to understand pore pressure evolution and natural fluid migration in similar geological settings. It suggests that fluid overpressure during lateral loadings developed as sudden pulses. This overpressure rapidly decreases if not sustained by on-going tectonic. In foreland settings, far-field tectonics can result in overpressure which induces significant fracturing in seal and reservoir rocks, therefore representing a key event for fluid migration. Consequently, it is critical to assess if such LPS events occurred throughout the basin geological history to decipher its pore pressure evolution, and subsequently the fluid migration. The timing and

amplitude of this shortening are however critically difficult to constrain from structural restoration, which advocates for further dedicated studies on the subject.

Acknowlegements

This study have been conducted in the framework of the IFPEN-Total project “Nomba”. The authors would like to thank Total Austral for providing the dataset. Nicolas Guy is thanked for his contribution on the numerical coupling and the preliminary study of the Neuquén basin. Adriana Traby is thanked for her help in handling the PSM software. Jean-Luc Rudkiewicz is thanked for discussion at different stages of the study.

References

Arregui, C., Carbone, O., Martinez, R., 2011. El grupo Cuyo (Jurasico temprano-medio) en la cuenca Neuquina, in: Relatorio del XVIII congreso geologico Argentino. Asociación Geológica Argentina Buenos Aires, Neuquén, p. 15.

Badessich, M.F., Hryb, D.E., Suarez, M., Mosse, L., Palermo, N., Pichon, S., Reynolds, L., 2016. Vaca Muerta Shale—Taming a Giant. Oilfield Review 28, 14.

Bemer, E., Vincké, O., Longuemare, P., 2004. Geomechanical Log Deduced from Porosity and Mineralogical Content. Oil & Gas Science and Technology - Rev. IFP 59, 405–426. https://doi.org/10.2516/ogst:2004028

Bouziat, A., Guy, N., Frey, J., Colombo, D., Colin, P., Cacas-Stentz, M.-C., Cornu, T., 2019. An Assessment of Stress States in Passive Margin Sediments: Iterative Hydro-Mechanical Simulations on Basin Models and Implications for Rock Failure Predictions. Geosciences 9, 469. https://doi.org/10.3390/geosciences9110469

Branellec, M., Callot, J.-P., Aubourg, C., Nivière, B., Ringenbach, J.-C., 2015. Matrix deformation in a basement-involved fold-and-thrust-belt: A case study in the central Andes, Malargüe (Argentina). Tectonophysics 658, 186–205. https://doi.org/10.1016/j.tecto.2015.07.022

Brüch, A., Colombo, D., Frey, J., Berthelon, J., Cacas-Stentz, M.-C., Cornu, T., 2020. Poro-elastoplastic constitutive law for coupling 3D geomechanics to classical petroleum system modeling. Presented at the 54rd U.S. Rock Mechanics/Geomechanics Symposium, American Rock Mechanics Association.

Burgreen-Chan, B., Meisling, K.E., Graham, S., 2016. Basin and petroleum system modelling of the East Coast Basin, New Zealand: a test of overpressure scenarios in a convergent margin. Basin Research 28, 536–567. https://doi.org/10.1111/bre.12121

Butler, R.W.H., Paton, D.A., 2010. Evaluating lateral compaction in deepwater fold and thrust belts: How much are we missing from “nature’s sandbox”? GSAT 4–10. https://doi.org/10.1130/GSATG77A.1

Chen, Y.-W., Wu, J., Suppe, J., 2019. Southward propagation of Nazca subduction along the Andes. Nature 565, 441–447. https://doi.org/10.1038/s41586-018-0860-1

Cobbold, P.R., Rodrigues, N., 2007. Seepage forces, important factors in the formation of horizontal hydraulic fractures and bedding-parallel fibrous veins ('beef' and 'cone-in-cone'). Geofluids 7, 313–322. https://doi.org/10.1111/j.1468-8123.2007.00183.x

Cobbold, P.R., Rossello, E.A., 2003. Aptian to recent compressional deformation, foothills of the Neuquén Basin, Argentina. Marine and Petroleum Geology 20, 429–443. https://doi.org/10.1016/S0264-8172(03)00077-1

Cobbold, P.R., Zanella, A., Rodrigues, N., Løseth, H., 2013. Bedding-parallel fibrous veins (beef and cone-in-cone): Worldwide occurrence and possible significance in terms of fluid overpressure, hydrocarbon generation and mineralization. Marine and Petroleum Geology 43, 1–20. https://doi.org/10.1016/j.marpetgeo.2013.01.010

Code_Aster [WWW Document], n.d. URL https://www.code-aster.org/spip.php?rubrique1 (accessed 6.4.20).

Couzens-Schultz, B.A., Azbel, K., 2014. Predicting pore pressure in active fold–thrust systems: An empirical model for the deepwater Sabah foldbelt. Journal of Structural Geology, Fluids and Structures in Fold and Thrust Belts with Recognition of the Work of David V. Wiltschko 69, 465–480. https://doi.org/10.1016/j.jsg.2014.07.013

Cristallini, E., Bottesi, G., Gavarrino, A., Rodríguez, L., Tomezzoli, R., Comeron, R., Kay, S.M., Ramos, V.A., 2006. Synrift geometry of the Neuquén Basin in northeastern Neuquén Province, Argentina, in: Evolution of An Andean Margin: Tectonic and Magmatic View from the Andes to the Neuquén Basin (35-39 S), Geological Society of America Special Papers. Boulder, Colo.; Geological Society of America; 1999, p. 147.

Di Giulio, D., Ronchi, A., Sanfilippo, A., Tiepolo, M., Pimentel, M., Ramos, V.A., 2012. Detrital zircon provenance from the Neuquén Basin (south-central Andes): Cretaceous geodynamic evolution and sedimentary response in a retroarc-foreland basin. Geology 40, 559–562. https://doi.org/10.1130/G33052.1

England, W.A., Mackenzie, A.S., Mann, D.M., Quigley, T.M., 1987. The movement and entrapment of petroleum fluids in the subsurface. Journal of the Geological Society 144, 327–347. https://doi.org/10.1144/gsjgs.144.2.0327

Evans, M.A., Fischer, M.P., 2012. On the distribution of fluids in folds: A review of controlling factors and processes. Journal of Structural Geology 44, 2–24. https://doi.org/10.1016/j.jsg.2012.08.003

Faille, I., Thibaut, M., Cacas, M.-C., Havé, P., Willien, F., Wolf, S., Agelas, L., Pegaz-Fiornet, S., 2014. Modeling Fluid Flow in Faulted Basins. Oil Gas Sci. Technol. – Rev. IFP Energies nouvelles 69, 529–553. https://doi.org/10.2516/ogst/2013204

Fennell, L.M., Naipauer, M., Borghi, P., Sagripanti, L., Pimentel, M., Folguera, A., 2020. Early Jurassic intraplate extension in west-central Argentina constrained by U-Pb SHRIMP dating: Implications for the opening of the Neuquén basin. Gondwana Research 87, 278–302. https://doi.org/10.1016/j.gr.2020.06.017

Garrido, A.C., 2011. El Grupo Neuquén (Cretácico Tardío) en la Cuenca Neuquina, in: Relatorio Del XVIII Congreso Geologico Argentino. Asociación Geológica Argentina Buenos Aires, Neuquén, pp. 231–244.

Guo, X., He, S., Liu, K., Zheng, L., 2011. Quantitative estimation of overpressure caused by oil generation in petroliferous basins. Organic Geochemistry 42, 1343–1350. https://doi.org/10.1016/j.orggeochem.2011.08.017

Guzmán, C., Cristallini, E., Bottesi, G., 2007. Contemporary stress orientations in the Andean retroarc between 34°S and 39°S from borehole breakout analysis. Tectonics 26. https://doi.org/10.1029/2006TC001958

Haddad, M., Du, J., Vidal-Gilbert, S., 2016. Integration of Dynamic Microseismic Data with a True 3D Modeling of Hydraulic Fracture Propagation in Vaca Muerta Shale. Presented at the SPE Hydraulic Fracturing Technology Conference, Society of Petroleum Engineers. https://doi.org/10.2118/179164-MS

Hansom, J., Lee, M.-K., 2005. Effects of hydrocarbon generation, basal heat flow and sediment compaction on overpressure development: a numerical study. Petroleum Geoscience 11, 353–360. https://doi.org/10.1144/1354-079304-651

Heine, C., 2007. ICONS - Formation and evolution of intracontinental basins (v.3) [WWW Document]. URL http://www.earthbyte.org/Resources/ICONS/ (accessed 5.12.20).

Horton, B.K., 2018. Tectonic Regimes of the Central and Southern Andes: Responses to Variations in Plate Coupling During Subduction. Tectonics 402–429. https://doi.org/10.1002/2017TC004624@10.1002/(ISSN)1944-9194.OROGENIC1

Hubbert, M.K., Rubey, W.W., 1959. Role of fluid pressure in mechanics of overthtrust faulting I. Mechanics of fluid-filled porous solid and its application to overthtrust faultig. GSA Bulletin 70, 115–166. https://doi.org/10.1130/0016-7606(1959)70[115:ROFPIM]2.0.CO;2

Kietzmann, D.A., Ambrosio, A.L., Suriano, J., Alonso, M.S., Tomassini, F.G., Depine, G., Repol, D., 2016. The Vaca Muerta–Quintuco system (Tithonian–Valanginian) in the Neuquén Basin, Argentina: A view from the outcrops in the Chos Malal fold and thrust belt. AAPG Bulletin 100, 743–771. https://doi.org/10.1306/02101615121

Kietzmann, D.A., Palma, R.M., Riccardi, A.C., Martín-Chivelet, J., López-Gómez, J., 2014. Sedimentology and sequence stratigraphy of a Tithonian–Valanginian carbonate ramp (Vaca Muerta Formation): A misunderstood exceptional source rock in the Southern Mendoza area of the Neuquén Basin, Argentina. Sedimentary Geology 302, 64–86. https://doi.org/10.1016/j.sedgeo.2014.01.002

Klotz, J., Angermann, D., Michel, G.W., Porth, R., Reigber, C., Reinking, J., Viramonte, J., Perdomo, R., Rios, V.H., Barrientos, S., Barriga, R., Cifuentes, O., 1999. GPS-derived Deformation of the Central Andes Including the 1995 Antofagasta Mw= 8.0 Earthquake, in: Sauber, J., Dmowska, R. (Eds.), Seismogenic and Tsunamigenic Processes in Shallow Subduction Zones, Pageoph Topical Volumes. Birkhäuser, Basel, pp. 709–730. https://doi.org/10.1007/978-3-0348-8679-6_14

Koyi, H.A., Sans, M., Teixell, A., Cotton, J., Zeyen, H., McClay, K.R., 2004. The Significance of Penetrative Strain in the Restoration of Shortened Layers—Insights from Sand Models and the Spanish Pyrenees, in: Thrust Tectonics and Hydrocarbon Systems, AAPG Memoirs. AAPG Special Volumes, pp. 207–222.

Larmier, S, 2020. Génération de fluides, migration et fracturation au sein des roches mères: cas de la formation de Vaca Muerta, bassin de Neuquén, Argentine (PhD Thesis) Le Mans Université. p. 507 Le Mans.

Lash, G.G., Engelder, T., 2005. An analysis of horizontal microcracking during catagenesis: Example from the Catskill delta complex. AAPG Bulletin 89, 1433–1449. https://doi.org/10.1306/05250504141

Lathrop, B.A., Burberry, C.M., 2017. Accommodation of penetrative strain during deformation above a ductile décollement. Lithosphere 9, 46–57. https://doi.org/10.1130/L558.1

Leanza, H.A., 2003. Las sedimentitas huitrinianas y rayosianas (Cretácico Inferior) en el ámbito central y meridional de la cuenca Neuquina, Argentina. (Technical Report). Servicio Geológico Minero Argentino. Instituto de Geología y Recursos Minerales.

Leanza, H.A., Sattler, F., Martínez, R., Carbone, O., 2011. La Formación Vaca Muerta y Equivalentes (Jurásico Tardío–Cretácico Temprano) en la Cuenca. Neuquina. Geología y Recursos Naturales de la Provincia del Neuquén, Neuquén. Buenos Aires: Asociación Geológica Argentina 113–129.

Lebinson, F., Turienzo, M., Sánchez, N., Araujo, V., D'Annunzio, M.C., Dimieri, L., 2018. The structure of the northern Agrio fold and thrust belt (37° 30'S), Neuquén Basin, Argentina. Andean Geology 45, 249–273.

Legarreta, L., Uliana, M.A., 1996. The Jurassic succession in west-central Argentina: stratal patterns, sequences and paleogeographic evolution. Palaeogeography, Palaeoclimatology, Palaeoecology 120, 303–330. https://doi.org/10.1016/0031-0182(95)00042-9

Legarreta, L., Villar, H.J., 2011. Geological and geochemical keys of the potential shale resources, Argentina Basins. In: AAPG Geosciences Technology Workshop - Unconventional Resources: Basics, Challenges, and Opportunities for New Frontier Plays, (Buenos Aires, Argentina, Search and Discovery Article # 80196)

Lorenz, J.C., Warpinski, N.R., Teufel, L.W., 1991. Regional Fractures I: A Mechanism for the Formation of Regional Fractures at Depth in Flat-Lying Reservoirs (1). AAPG Bulletin 75, 1714–1737.

Luijendijk, E., Gleeson, T., 2015. How well can we predict permeability in sedimentary basins? Deriving and evaluating porosity–permeability equations for noncemented sand and clay mixtures. Geofluids 15, 67–83. https://doi.org/10.1111/gfl.12115

Luo, Y., Liu, H., Zhao, Y., Wang, G., 2016. Effects of gas generation on stress states during burial and implications for natural fracture development. Journal of Natural Gas Science and Engineering 30, 295–304. https://doi.org/10.1016/j.jngse.2016.02.023

Mainguy, M., Longuemare, P., 2002. Coupling Fluid Flow and Rock Mechanics: Formulations of the Partial Coupling Between Reservoir and Geomechanical Simulators. Oil & Gas Science and Technology - Rev. IFP 57, 355–367. https://doi.org/10.2516/ogst:2002023

Messager, G., Nivière, B., Martinod, J., Lacan, P., Xavier, J.-P., 2010. Geomorphic evidence for Plio-Quaternary compression in the Andean foothills of the southern Neuquén Basin, Argentina. Tectonics 29. https://doi.org/10.1029/2009TC002609

Mitra, G., 1994. Strain variation in thrust sheets across the sevier fold-and-thrust belt (Idaho-Utah-Wyoming): implications for section restoration and wedge taper evolution. Journal of Structural Geology, Applications of Strain: From Microstructures to Orogenic Belts 16, 585–602. https://doi.org/10.1016/0191-8141(94)90099-X

Mosquera, A., Ramos, V.A., 2006. Intraplate deformation in the Neuquén Embayment (2006) Geological Society of America Special Paper, 407, in: Kay, S.M., Ramos, Victor A. (Eds.), Evolution of An Andean Margin: Tectonic and Magmatic View from the Andes to the Neuquén Basin (35-39 S), Geological Society of America Special Papers. pp. 97–123.

Mourgues, R., Cobbold, P.R., 2003. Some tectonic consequences of fluid overpressures and seepage forces as demonstrated by sandbox modelling. Tectonophysics 376, 75–97. https://doi.org/10.1016/S0040-1951(03)00348-2

Naipauer, M., Tunik, M., Marques, J.C., Vera, E.A.R., Vujovich, G.I., Pimentel, M.M., Ramos, V.A., 2015. U–Pb detrital zircon ages of Upper Jurassic continental successions: implications for the provenance and absolute age of the Jurassic–Cretaceous boundary in the Neuquén Basin. Geological Society, London, Special Publications 399, 131–154. https://doi.org/10.1144/SP399.1

Neumaier, M., Littke, R., Hantschel, T., Maerten, L., Joonnekindt, J.-P., Kukla, P., 2014. Integrated charge and seal assessment in the Monagas fold and thrust belt of VenezuelaIntegrated Charge and Seal Assessment, Monagas Fold and Thrust Belt, Venezuela. AAPG Bulletin 98, 1325–1350. https://doi.org/10.1306/01131412157

Obradors-Prats, J., Rouainia, M., Aplin, A.C., Crook, A.J.L., 2017. Hydromechanical Modeling of Stress, Pore Pressure, and Porosity Evolution in Fold-and-Thrust Belt Systems. Journal of Geophysical Research: Solid Earth 122, 9383–9403. https://doi.org/10.1002/2017JB014074

Osborne, M.J., Swarbrick, R.E., 1997. Mechanisms for Generating Overpressure in Sedimentary Basins: A Reevaluation. AAPG Bulletin 81, 1023–1041. https://doi.org/10.1306/522B49C9-1727-11D7-8645000102C1865D

Perrier, R., Quiblier, J., 1974. Thickness Changes in Sedimentary Layers During Compaction History; Methods for Quantitative Evaluation. AAPG Bulletin 58, 507–520. https://doi.org/10.1306/83D9142A-16C7-11D7-8645000102C1865D

Ramos, V.A., Folguera, A., 2005. Tectonic evolution of the Andes of Neuquén: constraints derived from the magmatic arc and foreland deformation. Geological Society, London, Special Publications 252, 15–35. https://doi.org/10.1144/GSL.SP.2005.252.01.02

Ramos, V.A., Kay, S.M., 2006. Overview of the tectonic evolution of the Southern Central Andes of Mendoza and Neuquen (35°-39°S latitude), in: Kay, S.M., Ramos, V. A. (Eds.), Evolution of an Andean Margin: A Tectonic and Magmatic View from the Andes to the Neuquén Basin (35°-39°S Lat), Geological Society of America Special Papers. Geological Society of America, pp. 1–17.

Ravier, E., Martinez, M., Pellenard, P., Zanella, A., Tupinier, L., 2020. The milankovitch fingerprint on the distribution and thickness of bedding-parallel veins (beef) in source rocks. Marine and Petroleum Geology 122, 104643. https://doi.org/10.1016/j.marpetgeo.2020.104643

Robion, P., Grelaud, S., Frizon de Lamotte, D., 2007. Pre-folding magnetic fabrics in fold-and-thrust belts: Why the apparent internal deformation of the sedimentary rocks from the Minervois basin (NE — Pyrenees, France) is so high compared to the Potwar basin (SW — Himalaya, Pakistan)? Sedimentary Geology, Deformation of soft sediments in nature and laboratory 196, 181–200. https://doi.org/10.1016/j.sedgeo.2006.08.007

Rodrigues, N., Cobbold, P.R., Loseth, H., Ruffet, G., 2009. Widespread bedding-parallel veins of fibrous calcite ('beef') in a mature source rock (Vaca Muerta Fm, Neuquén Basin, Argentina): evidence for overpressure and horizontal compression. Journal of the Geological Society 166, 695–709. https://doi.org/10.1144/0016-76492008-111

Rojas Vera, E.A., Folguera, A., Zamora Valcarce, G., Bottesi, G., Ramos, V.A., 2014. Structure and development of the Andean system between 36° and 39°S. Journal of Geodynamics 73, 34–52. https://doi.org/10.1016/j.jog.2013.09.001

Rojas Vera, E.A., Mescua, J., Folguera, A., Becker, T.P., Sagripanti, L., Fennell, L., Orts, D., Ramos, V.A., 2015. Evolution of the Chos Malal and Agrio fold and thrust belts, Andes of Neuquén: Insights from structural analysis and apatite fission track dating. Journal of South American Earth Sciences, Tectonics of the Argentine and Chilean Andes 64, 418–433. https://doi.org/10.1016/j.jsames.2015.10.001

Roure, F., Andriessen, P., Callot, J.P., Faure, J.L., Ferket, H., Gonzales, E., Guilhaumou, N., Lacombe, O., Malandain, J., Sassi, W., Schneider, F., Swennen, R., Vilasi, N., 2010. The use of palaeo-thermo-barometers and coupled thermal, fluid flow and pore-fluid pressure modelling for hydrocarbon and reservoir prediction in fold and thrust belts. Geological Society, London, Special Publications 348, 87–114. https://doi.org/10.1144/SP348.6

Roure, F., Swennen, R., Schneider, F., Faure, J.L., Ferket, H., Guilhaumou, N., Osadetz, K., Robion, P., Vandeginste, V., 2005. Incidence and Importance of Tectonics and Natural Fluid Migration on Reservoir Evolution in Foreland Fold-And-Thrust Belts. Oil & Gas Science and Technology - Rev. IFP 60, 67–106. https://doi.org/10.2516/ogst:2005006

Sagasti, G., Foster, M., Hryb, D., Ortiz, A., Lazzari, V., 2014. Understanding Geological Heterogeneity to Customize Field Development: An Example from the Vaca Muerta Unconventional Play, Argentina, in: Unconventional Resources Technology Conference (URTeC). Unconventional Resources Technology Conference (URTEC), Denver, Colorado, USA.

Sagripanti, L., Colavitto, B., Astort, A., Folguera, A., 2020. Quaternary Deformation in the Neuquén Basin, Explained by the Interaction Between Mantle Dynamics and Tectonics. In : Opening and Closure of the Neuquén Basin in the Southern Andes. Springer, Cham, 2020. p. 485-499.

Sánchez, N.P., Coutand, I., Turienzo, M., Lebinson, F., Araujo, V., Dimieri, L., 2018. Tectonic Evolution of the Chos Malal Fold-and-Thrust Belt (Neuquén Basin, Argentina) From (U-Th)/He and Fission Track Thermochronometry. Tectonics 37, 1907–1929. https://doi.org/10.1029/2018TC004981

Sans, M., Vergés, J., Gomis, E., Parés, J.M., Schiattarella, M., Travé, A., Calvet, F., Santanach, P., Doulcet, A., 2003. Layer parallel shortening in salt-detached folds: constraint on cross-section restoration. Tectonophysics 372, 85–104. https://doi.org/10.1016/S0040-1951(03)00233-6

Schneider, F., Wolf, S., Faille, I., Pot, D., 2000. A 3d Basin Model for Hydrocarbon Potential Evaluation: Application to Congo Offshore. Oil & Gas Science and Technology - Rev. IFP 55, 3–13. https://doi.org/10.2516/ogst:2000001

Schwarz, E., Howell, J.A., 2005. Sedimentary evolution and depositional architecture of a lowstand sequence set: the Lower Cretaceous Mulichinco Formation, Neuquén Basin, Argentina. Geological Society, London, Special Publications 252, 109–138. https://doi.org/10.1144/GSL.SP.2005.252.01.06

Sibson, R.H., 2003. Brittle-failure controls on maximum sustainable overpressure in different tectonic regimes. AAPG Bulletin 87, 901–908. https://doi.org/10.1306/01290300181

Spalletti, L.A., Veiga, G.D., Schwarz, E., Leanza, H.A., Arregui, C., 2011. La Formación Agrio (Cretácico Temprano) en la Cuenca Neuquina, in: Relatorio Del XVIII Congreso Geológico Argentino. Asociación Geológica Argentina Buenos Aires, pp. 145–160.

Spacapan, J.B., Palma, J.O., Galland, O., Manceda, R., Rocha, E., D'Odorico, A., Leanza, H.A., 2018. Thermal impact of igneous sill-complexes on organic-rich formations and implications for petroleum systems: A case study in the northern Neuquén Basin, Argentina. Marine and Petroleum Geology 91, 519–531. https://doi.org/10.1016/j.marpetgeo.2018.01.018

Sylwan, C., 2014. Source rock properties of Vaca Muerta Formation, Neuquina Basin, Argentina, Simposio de Recursos No Convencionales. In: IX Congreso Argentino de Exploración y Desarrollo de Hidrocarburos. IAPG, Mendoza, Argentina.

Swarbrick, R.E., Yardley, G.S., Osborne, M.J., 2001. Comparision of Overpressure Magnitude Resulting from the Main Generating Mechanisms, in: Huffman, A., Bowers, G. (Eds.), Pressure Regimes in Sedimentary Basins and Their Prediction, AAPG Memoirs. AAPG Special Volumes, pp. 1–12.

Tavani, S., Storti, F., Lacombe, O., Corradetti, A., Muñoz, J.A., Mazzoli, S., 2015. A review of deformation pattern templates in foreland basin systems and fold-and-thrust belts: Implications for the state of stress in the frontal regions of thrust wedges. Earth-Science Reviews 141, 82–104. https://doi.org/10.1016/j.earscirev.2014.11.013

Tingay, M.R.P., Morley, C.K., Laird, A., Limpornpipat, O., Krisadasima, K., Pabchanda, S., Macintyre, H.R., 2013. Evidence for overpressure generation by kerogen-to-gas maturation in the northern Malay BasinOrigin of Overpressure in the Northern Malay Basin. AAPG Bulletin 97, 639–672. https://doi.org/10.1306/09041212032

Tissot, B.P., Pelet, R., Ungerer, P., 1987. Thermal History of Sedimentary Basins, Maturation Indices, and Kinetics of Oil and Gas Generation. AAPG Bulletin 71, 1445–1466. https://doi.org/10.1306/703C80E7-1707-11D7-8645000102C1865D

Tuncay, K., Ortoleva, P., 2004. Quantitative basin modeling: present state and future developments towards predictability. Geofluids 4, 23–39. https://doi.org/10.1111/j.1468-8123.2004.00064.x

Tunik, M., Folguera, A., Naipauer, M., Pimentel, M., Ramos, V.A., 2010. Early uplift and orogenic deformation in the Neuquén Basin: Constraints on the Andean uplift from U–Pb and Hf isotopic data of detrital zircons. Tectonophysics 489, 258–273. https://doi.org/10.1016/j.tecto.2010.04.017

Turcotte, D.L., Schubert, G., 2002. Geodynamics. Cambridge University Press.

Ukar, E., Lopez, R.G., Gale, J.F.W., Laubach, S.E., Manceda, R., 2017. New type of kinematic indicator in bed-parallel veins, Late Jurassic–Early Cretaceous Vaca Muerta Formation, Argentina: E-W shortening during Late Cretaceous vein opening. Journal of Structural Geology 104, 31–47. https://doi.org/10.1016/j.jsg.2017.09.014

Veiga, G.D., Schwarz, E., Spalletti, L.A., 2011. Stratigraphic analysis of the Lotena Formation (upper Callovian-lower Oxfordian) in central Neuquen Basin, Argentina. Andean Geology 38, 171–197. https://doi.org/10.5027/andgeoV38n1-a10

Vergani, G.D., Tankard, A.J., H.J. Belotti, Welsink, H.J., 1995. Tectonic Evolution and Paleogeography of the Neuquén Basin, Argentina, in: Tankard, A.J., Suarez Soruco, R., Welsink, H.J. (Eds.), Petroleum Basins of South America, AAPG Memoirs. AAPG, pp. 383–402.

Weger, R.J., Murray, S.T., McNeill, D.F., Swart, P.K., Eberli, G.P., Blanco, L.R., Tenaglia, M., Rueda, L.E., 2019. Paleothermometry and distribution of calcite beef in the Vaca Muerta Formation, Neuquén Basin, Argentina. AAPG Bulletin 103, 931–950. https://doi.org/10.1306/10021817384

Woillez, M.-N., Souque, C., Rudkiewicz, J.-L., Willien, F., Cornu, T., 2017. Insights in Fault Flow Behaviour from Onshore Nigeria Petroleum System Modelling. Oil & Gas Science and Technology - Rev. IFP Energies nouvelles 72, 31. https://doi.org/10.2516/ogst/2017029

Wood, D.M., 1990. Soil Behaviour and Critical State Soil Mechanics. Cambridge University Press.

Zamora-Valcarce, G., 2007. Estructura y Cinemática de la faja plegada del Agrio, Cuenca Neuquina (PhD Thesis). University of Buenos Aires, Buenos Aires, Argentina.

Zamora-Valcarce, G., Zapata, T., 2015. Building a valid structural model in a triangle zone: An example from the Neuquén fold and thrust belt, Argentina. Interpretation 3, SAA117–SAA131. https://doi.org/10.1190/INT-2015-0014.1

Zamora-Valcarce, G., Zapata, T., del Pino, D., Ansa, A., 2006. Structural evolution and magmatic characteristics of the Agrio fold-and-thrust belt, in: Kay, S.M., Ramos, V.A. (Eds.), Evolution of an Andean Margin: A Tectonic and Magmatic View from the Andes to the Neuquén Basin (35°-39°S Lat), Geological Society of America Special Papers. Boulder, Colo.; Geological Society of America; 1999, pp. 125–145.

Zamora-Valcarce, G., Zapata, T., Ramos, V.A., Rodríguez, F., Bernardo, L.M., 2009. Evolucion tectonica del frente Andino en Neuquen. Revista de la Asociacon Geologica Argentina 65, 192–203.

Zanella, A., Cobbold, P.R., Ruffet, G., Leanza, H.A., 2015. Geological evidence for fluid overpressure, hydraulic fracturing and strong heating during maturation and migration of hydrocarbons in Mesozoic rocks of the northern Neuquén Basin, Mendoza Province, Argentina. Journal of South American Earth Sciences 62, 229–242. https://doi.org/10.1016/j.jsames.2015.06.006

Zanella, A., Cobbold, P.R., Rodrigues, N., Loseth, H., Jolivet, M., Gouttefangeas, F., Chew, D., 2020. Source rocks in foreland basins: a preferential context for the development of natural hydraulic fractures. AAPG Bulletin, ahead of print. https://doi.org/10.1306/08122018162

Zapata, T., Folguera, A., 2005. Tectonic evolution of the Andean Fold and Thrust Belt of the southern Neuquén Basin, Argentina. Geological Society, London, Special Publications 252, 37–56. https://doi.org/10.1144/GSL.SP.2005.252.01.03

Zavala, C., Ponce, J.J., 2011. La Formación Rayoso (Cretácico Temprano) en la Cuenca Neuquina, in: XVIII Congreso Geol Ógico Argentino, Neuquén. Asociación Geológica Argentina Buenos Aires, pp. 2–6.

Zoback, M.D., 2010. Reservoir Geomechanics. Cambridge University Press.

Zoback, M.L., Zoback, M.D., Adams, J., Assumpção, M., Bell, S., Bergman, E.A., Blümling, P., Brereton, N.R., Denham, D., Ding, J., Fuchs, K., Gay, N., Gregersen, S., Gupta, H.K., Gvishiani, A., Jacob, K., Klein, R., Knoll, P., Magee, M., Mercier, J.L., Müller, B.C., Paquin, C., Rajendran, K., Stephansson, O., Suarez, G., Suter, M., Udias, A., Xu, Z.H., Zhizhin, M., 1989. Global patterns of tectonic stress. Nature 341, 291–298. https://doi.org/10.1038/341291a0

Supplementary materials

Lithology	(a) Thermal parameters				(b) Petrophysical parameters									(c) Mechanical parameters			
					Compaction							*Permeability*		*Elastic*		*Plastic*	
	S.m.c	T.D	H.C.	R.P.	ρs	φr	φa	φb	σa	σb	E_{obs}	Sp.surface	K An.	E	ν	Pt	M
Sandstone	6.32	0.004	700	5e-7	2675	0.01	0.44	0	30	0	10000	4.e6	1	9200	0.24	0.25	1.2
70%-30% sandstone-shale	4.56	0.0032	740	9.5e-7	2665	0.01	0.49	0	28	0	1000	1.7e6	1	7500			
50%-50% sandstone-shale	3.67	0.0027	765	1.3e-6	2660	0.01	0.54	0	13.6	0	100000	1.e7	0.5	5700			
30%-70% sandstone-shale	2.95	0.0023	790	1.5e-6	2650	0.01	0.54	0	20	0	10000	1.2e7	1	5250			
Shale	2.37	0.002	815	1.9e-6	2654	0.04	0.56	0	16	0	20000	N/A	0.2	4500			
Evaporites	4.76	0.001	550	9.e-8	2700	0.01	0.29	0	40	0	10000	5.e7	1	1300			
Limestone	3.57	0.003	795	6.2e-7	2710	0.04	0.56	0	20	0	50000	4.e7	0.1	9000			
Upper crust	3	0.001	1150	3.5e-6	N/A												
Lower crust	2	0.001	1030	7e-7	N/A												
Upper Mantle	3	0	1200	0	N/A												
Water	N/A		3620	N/A	Water Salinity (g/L): 126.004, Water compressibility (1/L): 4.5e-5									N/A			

Table 1: Thermal, petrophysical and mechanical parameters used in the simulation. (a) Thermal parameters. S.m.c: Surface matrix conductivity W/(m.°C)), T.D.: Temperature Dependendy (1/°C), H.C.: Heat Capacity (J/(kg.°C)), R.P.: Radiogenic Production (W/m^3). (b) Petrophysical parameters. ρs: solid volumic mass (kg/m^3), φr: residual porosity, φa: observed porosity a, φb: observed porosity b, σa: observed sigma a (MPa), σb: observed sigma b (MPa), E_{obs}: Observed elasticity, for the PSM simulation only (MPa), Sp. Surface : Specific surface of the Kozeni Carman porosity-permeability law (1/m), K An.: vertical

anisotropy multiplier. (c) Mechanical parameters. E: Young Modulus (MPa), v: poisson ratio, Pt: tensile intercept of the yield surface with the hydrostatic axis (MPa), M: slope of the Critical State Line.